EARTH SCIENCES
RESEARCH JOURNAL
Earth Sci. Res. J. Vol. 29, No. 2 (June, 2025): 113 - 130

UNIVERSIDAD NACIONAL DE COLOMBIA

GEOLOGY

Mineralogy and geochemistry of stratabound Cu (±Ag) deposits: Insights from the "La Quinta" Formation, northern Colombia

Andrés Felipe González-Durán[1]*, Juan Carlos Molano-Mendoza[1], María Janeth Sepúlveda-Ospina[2], Néstor Alfredo Cano-Hernández[1], Nathalia Marcela Guerrero-Higuera[1], Luis Alejandro Contreras-Palencia[1].

1. Departamento de geociencias, Universidad Nacional de Colombia, Bogotá.
anfgonzalezdu@unal.edu.co; jcmolanom@unal.edu.co; ncanoh@unal.edu.co; nmguerreroh@unal.edu.co; lcontrerasp@unal.edu.co

2. Servicio Geológico Colombiano. mjsepulveda@sgc.gov.co

*Corresponding author: anfgonzalezdu@unal.edu.co

ABSTRACT

The "La Quinta" Formation is a volcano-sedimentary unit formed by continental, oxidized redbeds interlayered with subaerial felsic-to-mafic lava flows. This lithostratigraphic unit, which outcrops in the Perijá Range (northern Colombia), hosts two different stratabound Cu (±Ag) mineralization styles: basalt-hosted and sediment-hosted. The former style of mineralization comprises native copper and silver, along with minor amounts of Cu-sulfides hosted flow-top mafic lavas. Conversely, the latter mineralization style primarily consists of chalcopyrite, bornite, and digenite hosted by sedimentary strata. Electron Probe Micro-Analyzer (EPMA) analyses indicate that Cu-sulfides in both mineralization styles host silver. On the other hand, the assessment of mineral assemblages suggests a low-temperature and epigenetic origin for the Cu (±Ag) mineralization in both basaltic flows and sedimentary strata. Also, the identified hydrothermal alterations comprise four distinct stages occurring in the next chronological order: (1) Na-rich, (2) K-rich, (3) Ca-Si-rich, and (4) Ca-CO_2-rich alterations. The hypogene ore minerals were observed paragenetically associated with the Ca-Si-rich alteration. In sediment-hosted deposits, mineralization is closely associated with charcoal clasts and possibly pyrobitumen. These forms of organic matter may serve as possible sources of reduced sulfur, which may trigger the precipitation of Cu-sulfides upon contact with mineralizing fluids. Additionally, a strong alteration involving Ca, Mg, Na, K, and Fe is evidenced by lithogeochemistry analyses. These analyses also suggest a depletion of K, Rb, and Cs contents in the samples with hydrothermal alteration, and also evidence no significant variation of Si and Rare Earth Elements (REE), implying these elements remained immobile during the different stages of hydrothermal alteration. Despite the above, most major and trace elements evidence a wide range of variation, implying that the alteration reactions were primarily controlled by lithological factors. Moreover, the supergene oxidation of hypogene ore minerals resulted in the formation of spionkopite, anilite, covellite, and other secondary Cu-bearing minerals. Overall, the characteristics of the Cu (±Ag) deposits hosted in the "La Quinta" Formation are similar to those described for Chilean Manto-type Cu deposits and Volcanic Redbed Cu deposits.

Keywords: Perijá Range; copper sulfides; digenite; anilite; spionkopite; organic matter.

Mineralogía y geoquímica de depósitos estratoligados Cu (±Ag): Perspectivas de la Formación "La Quinta", norte de Colombia

RESUMEN

La Formación "La Quinta" es una unidad volcano-sedimentaria formada por capas rojas continentales, oxidadas e interestratificadas con flujos lávicos subaéreos de composición félsica a máfica. Esta unidad litoestratigráfica que aflora en la Serranía del Perijá (norte de Colombia), hospeda dos diferentes estilos de mineralización estratoligada Cu (±Ag): Hospedada en basaltos y hospedada en sedimentos. El primer estilo de mineralización comprende cobre y plata nativos, junto con cantidades menores de sulfuros de Cu hospedados en flujos lávicos máficos. Por el contrario, el segundo estilo de mineralización consiste principalmente de calcopirita, bornita, y digenita hospedadas en estratos sedimentarios. Microanálisis con sonda electrónica (EPMA) indican que los sulfuros de Cu presentes en ambos estilos de mineralización hospedan plata. Por otro lado, la evaluación de ensambles minerales sugiere un origen de baja temperatura y epigenético para la mineralización Cu (±Ag) en los flujos basálticos y estratos sedimentarios. También, las alteraciones hidrotermales identificadas comprenden cuatro diferentes etapas que ocurren en el siguiente orden cronológico: (1) Alteración rica en Na, (2) alteración rica en K, (3) alteración rica en Ca-Si y, (4) alteración rica en Ca-CO_2. Los minerales de mena hipógenos fueron observados paragenéticamente asociados con la alteración enriquecida en Ca-Si. En los depósitos hospedados en sedimentos, la mineralización se encuentra estrechamente asociada con clastos de carbón y posiblemente pirobitumen. Estas formas de materia orgánica podrían servir como posibles fuentes de azufre reducido, las cuales podrían desencadenar la precipitación de sulfuros de Cu al entrar en contacto con fluidos mineralizantes. Adicionalmente, una fuerte alteración que involucra Ca, Mg, Na, y Fe es evidenciada mediante análisis litogeoquímicos. Estos análisis también sugieren una disminución en los contenidos de K, Rb y Cs en las muestras con alteración hidrotermal, y también evidencian una variación insignificante del Si y tierras raras (REE), lo que implica que estos elementos permanecieron inmóviles durante las diferentes etapas de alteración hidrotermal. A pesar de lo anterior, la mayor parte de elementos mayores y traza evidencian un amplio rango de variación, lo que implica que las reacciones de alteración fueron principalmente controladas por factores litológicos. Además, la oxidación supérgena de minerales de mena hipogénicos resultó en la formación de spionkopita, anilita y covelita, además de otros minerales secundarios de Cu. En general, las características de los depósitos Cu (±Ag) hospedados en la Formación "La Quinta" son similares a aquellas descritas para depósitos cupríferos tipo Manto Chileno y Volcanic Redbed.

Palabras clave: Serranía del Perijá; sulfuros de cobre; digenita; anilita; spionkopita; materia orgánica.

Record
Manuscript received: 07/03/2024
Accepted for publication: 16/06/2025

How to cite this item:
Gonzalez Duran, A. F., Molano Mendoza, J. C., Sepulveda Ospina, M. J., Cano Hernandez, N. A., Guerrero Higuera, N. M., & Contreras Palencia, L. A. (2025). Mineralogy and geochemistry of stratabound Cu (±Ag) deposits: Insights from the "La Quinta" Formation, northern Colombia. *Earth Sciences Research Journal, 29*(2), 113-130. https://doi.org/10.15446/esrj.v29n2.113381

1. Introduction

Copper and silver are essential materials in the manufacturing of renewable energy technologies due to their chemical properties, which make them ideal for many electrical and electronic applications (IEA., 2021; Apergis & Apergis, 2019). Mining these metals offers an opportunity to boost Colombia's economy. However, mineral deposits with copper and silver remain underexplored within the country.

Exploration efforts and advancements in knowledge have primarily focused on Porphyry and Epithermal deposits, particularly those belonging to the Middle Cauca Belt. This Miocene magmatic arc hosts Porphyry Au-Cu-(Mo) and Intermediate Sulfidation Au-Ag-Zn deposits (Sillitoe et al., 1982; Loboguerrero, 2003; Sillitoe, 2008; Bartos, 2017).

Other well-known copper- and silver-hosting deposits in Colombia include Skarns, Volcanogenic Massive Sulfide (VMS) and Iron Oxide Copper Gold (IOCG) deposits. Occurrences of Cu (Au-Ag) Skarns are associated with the contact between the Jurassic Ibagué Batholith and Triassic limestones and conglomerates (Alvarán et al., 2011; Shaw et al., 2019). Cu (Au-Zn-Ag) VMS deposits have been identified throughout the basaltic and marine sedimentary units of the Cañas Gordas Terrane (Shaw, 2014; Shaw et al., 2019; Murillo-Bedoya, 2020) and IOCG-style mineralization has been proposed to occur at the El Alacrán Cu-Au deposits hosted in the Calima Terrane in the Western Cordillera (Sillitoe, 2018; Manco, 2020).

Conversely, the nature of Colombian stratabound Cu-Ag deposits remains not yet fully understood. Volcanic- and sediment-hosted stratabound Cu (±Ag) deposits have been widely documented within the "La Quinta" Formation in the Perijá Range, Northern Colombia. (Wokittel, 1957; Champetier et al., 1961; Pagnacco, 1963; Viteri, 1978; Maze, 1984; Rodríguez, 1986; Jiménez, 2010; Ortega et al., 2012a, 2012b; Cardeño-Villegas et al., 2015; Manco-Jaraba et al., 2019). However, the origin of the widespread native copper mineralization at the "La Quinta" Formation (Wokittel, 1957; Ortega et al., 2012) and the occurrence of copper and silver minerals within both sedimentary and volcanic units have received limited research attention. Consequently, this study aims to address the origin of copper and silver minerals hosted in the "La Quinta" Formation through detailed field observations, mineral characterization, and geochemistry.

2. Geological Setting

The Perijá Range, representing the northernmost part of the Colombian Eastern Cordillera, acts as an uplift between the Cesar – Ranchería and Maracaibo basins (Fig. 1A). It is bordered northwards by the Oca fault system, westwards by the Cerrejón fault, and eastwards by the Perijá- El Tigre faults (Fig. 1B) (Miller, 1962; Colmenares et al., 2007; Nova et al., 2012). The Perijá mountain range follows a N30E trend (Ujueta & Llinás, 1990), and its inner structure is primarily controlled by reverse faults such as the Media Luna and Manaure systems (Fig. 1B, C) (Ujueta & Llinás,1990; Geoestudios, 2006).

The study area is in the western foothills of the Perijá Range (Fig. 1B, C). The lithological units in this region span from the Paleozoic to the Quaternary. The oldest units comprise Cambro-Ordovician phyllites and quartzites, overlaid by Devonian-Carboniferous sediments comprising conglomeratic and lithic sandstones, interbedded with mudstones (Champetier et al., 1961; Radelli, 1962; Forero, 1970; Colmenares et al., 2007; Pastor-Chacón et al., 2013). Minor Triassic porphyritic andesites have been reported by Tschanz et al. (1969) and Colmenares et al. (2007). However, the area is dominated by the "La Quinta" Formation, a thick succession of Jurassic volcano-sedimentary strata, ranging from 1600 to 3000 m in thickness (Maze, 1984; Arias & Morales, 1999; Gómez et al., 2010). Maze (1984), further divides the "La Quinta" Formation into three sections (Fig. 2):

- Lower section (~800 m thick): Comprises a thick sequence dominated by fine to medium-grained, dark red-brown arkoses with occasional volcanic rocks. Minor coarse-grained, pale green, arkosic sandstones, usually contain plant fragments and charcoal clasts. In the lower part, thin limestone beds, lenses, concretions, and fossil-bearing horizons can be found. Preserved conchostracan fossils are abundant within one of these basal limestone horizons.
- Transition zone (~100 m thick): Includes basaltic andesite flows from 1 m to greater than 20 m, which are overlain by sequences of fine to coarse-grained, dark red-brown arkoses and red to black mudstones. Minor green beds may contain various types of fossils, including estherids, vertebrate remains, carbon pieces, and large plant fragments. Calcareous concretions, nodules, and lenses are less common than in the lower section.
- Upper part (~800 m thick): Comprises interbedded lithologies including dark red to dark-brown coarse-grained arkoses, conglomerates, pinkish felsic ash layers, and tuffs. Light-green sandstones containing plant fragments can also be found. Basaltic-andesite flows from 1 to 15 m in thickness, are interbedded with red beds on top. The flow top portions are usually vesicular and may contain native copper mineralization. Additionally, many felsic to intermediate ash layers, welded tuffs, and flows are commonly interbedded with the mafic flows and arkoses.

The lithological descriptions provided by Maze (1984) closely resemble those reported for the "La Quinta" Formation, near the study area, by Wokittel (1957), Pagnaco (1963), Champetier et al. (1961), Radelli (1962), and Gómez et al. (2010).

The volcanic- and sediment-hosted Cu (±Ag) mineralization in the "La Quinta" Formation is predominantly stratabound and occasionally stratiform. The term "stratabound" denotes the preferential linkage of mineralization with specific stratigraphic levels. On the other hand, "stratiform" indicates that mineralization exhibits the overall morphology of sedimentary strata. Stratiform mineralized bodies always crosscut the stratification (Wilkinson, 2014).

Additionally, U-Pb zircon dating of volcanic rocks in the "La Quinta" Formation suggests an age range of 191–164 Ma for this unit (Jiménez, 2010; González et al., 2015; Rodríguez-García & Obando, 2020). This aligns with the Jurassic ages indicated by the fossil record (Forero, 1970; Maze, 1984). According to Kammer & Mojica (1995), Maze (1984), and Rodríguez-García & Obando (2020), the "La Quinta" Formation originated from the accumulation of sediments in a Jurassic basin bordered by normal faults. Within this basin, continental sediments were deposited with a significant contribution of volcanic material resulting from intense calc-alkaline magmatism in a continental margin arc setting. Due to the extension of Jurassic strata along the Colombian Andes, the "La Quinta" Formation has been correlated with the "Guatapurí" and "Saldaña" Formations (Tschanz et al., 1969; Cediel et al., 1981; Colmenares et al., 2007).

The "La Quinta" Formation is unconformably overlain by Cretaceous strata, composed of limestones and mudstones from the "Cogollo" Group and "Rionegro" Formation (Forero, 1970; Maze, 1984; Gómez et al., 2010). Massive alluvial fans and terraces occur in the foothills area, corresponding to recent (Quaternary) deposits (Fig. 1C) (Arias & Morales, 1999; Hernández, 2003; Gómez et al., 2010).

3. Methods

Mineralized outcrop rock samples were collected from different zones across the western foothills of the Perijá Range (Fig. 1C). Petrographic description of 65 of these samples was carried out under reflected and transmitted light using an Olympus BX41 microscope at the Mineral Characterization Laboratory of the Universidad Nacional de Colombia, Bogotá. The abbreviations for the names of minerals displayed in the microphotographs (Fig. 4, 5, 6, 7) are after Warr (2021).

Detailed mineral chemistry analyses were performed on carbon-coated polished thin sections through Electron Probe Micro-Analyzer (EPMA) using a JEOL superprobe JXA-8230 at the Universidad Nacional de Colombia. EPMA analyses were done at an accelerating voltage of 15 kV and beam current of 20 nA, and included the detection of S, Cu, Fe, and Ag contents in selected ore minerals.

Additionally, lithogeochemical assessments of 6 outcrop rock samples were conducted at ALS laboratories in Canada. These employed Inductively Coupled Plasma - Atomic Emission Spectroscopy (ICP-AES) and Inductively Coupled Plasma - Mass Spectrometry (ICP-MS) techniques following lithium borate fusion and multi-acid digestion for major and trace element detection. Analyzed elements comprise major oxides (SiO_2, Al_2O_3, Fe_2O_3, CaO, MgO, Na_2O, K_2O, Cr_2O_3, TiO_2, MnO, P_2O_5, SrO, BaO) and trace elements (Ba, Cr, Cs, Ga, Rb, Sn, Sr, Th, U, V, W, Zr, Nb, Ta, As, Co, Li, Mo, Ni, Pb, Zn, Hf, Cu), including Rare Earth Elements (La, Ce, Pr, Nd, Sm, Eu, Gd, Tb, Dy, Ho, Er, Tm, Yb, Lu, Sc, Y).

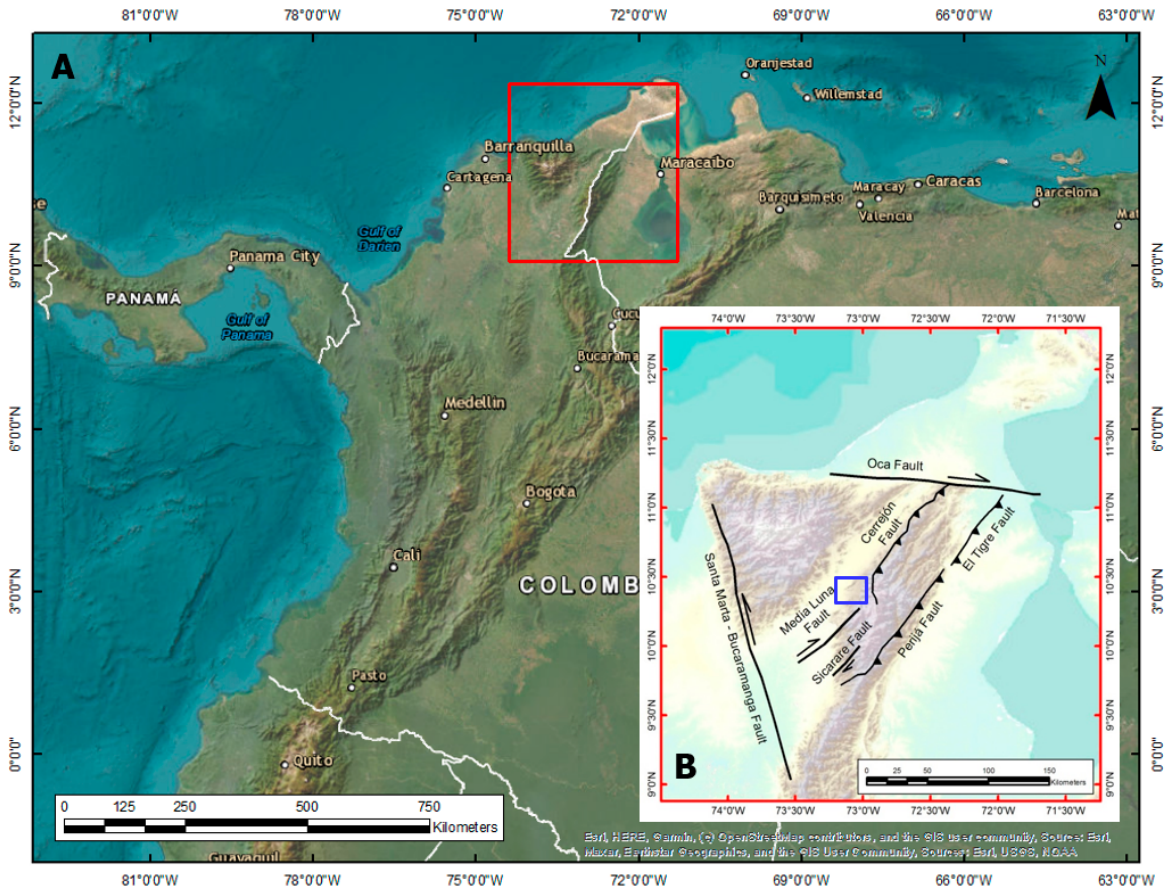

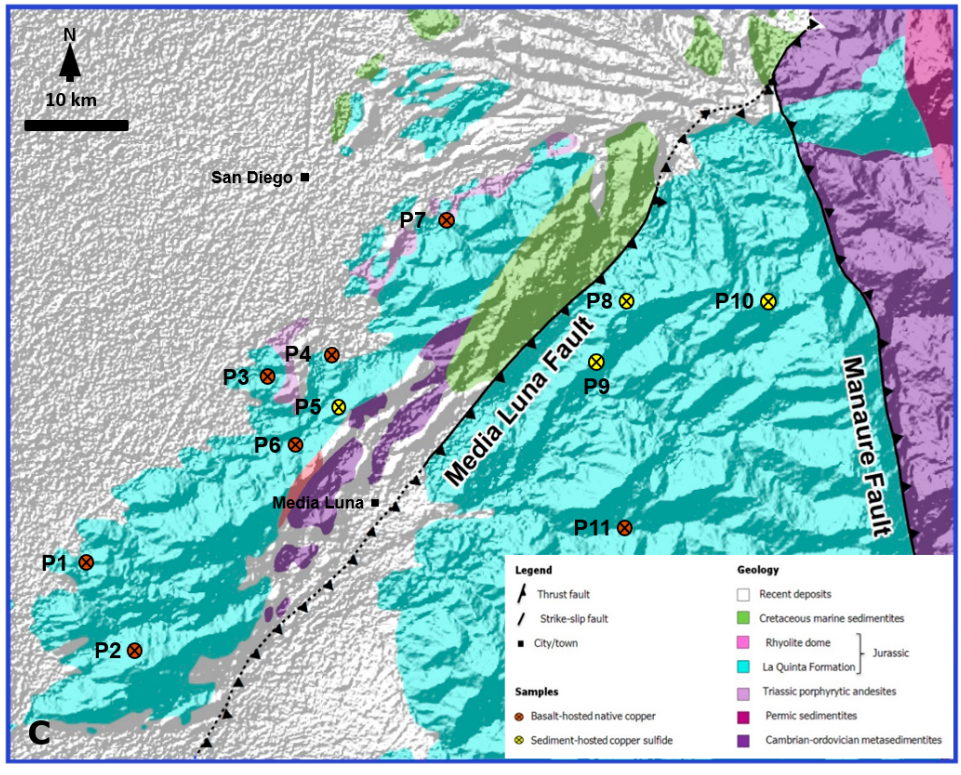

Figure 1. A) Map showing the location of the Santa Marta Massif and the northernmost segment of the Colombian Eastern Cordillera. **B)** Schematic map of northern Colombia displaying the principal regional faults as described by Colmenares et al. (2007). The study area is highlighted in a blue square. **C)** Map of the local geology and sampling distribution within the study area. The geological basemap was taken from the 34 – Agustín Codazzi geological map sheet from Colmenares et al. (2007).

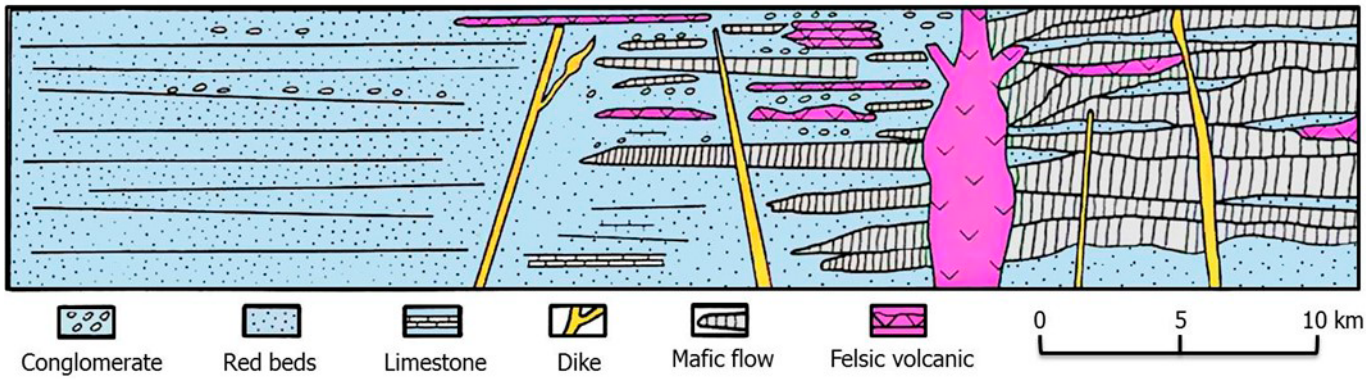

Figure 2. Schematic cross section of the "La Quinta" Formation (Maze,1984). Colors were added to facilitate interpretation.

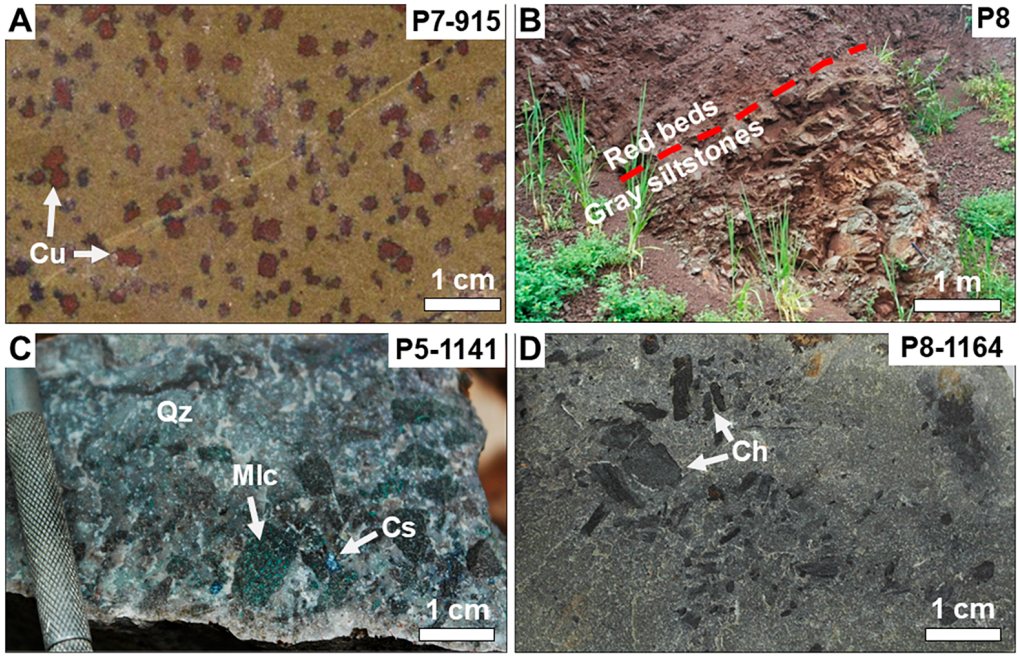

Figure 3. A) Vesicular basalt containing native copper (Cu) and displaying intense hydrothermal alteration. The sample location is P7 (Fig. 1C). **B)** Sharp contact between red beds and copper-bearing siltstones. The location of the outcrop is P8 (Fig.1C). **C)** Hydrothermal breccia with quartz (Qz), malachite (Mlc), and Cu-sulfides (Cs). The sample locality is P5 (Fig.1C). **D)** Copper-bearing siltstones containing charcoal (Ch) angular clasts. This sample exhibits silicification and was collected at locality P8 (Fig.1C).

4. Results

Mineralization styles

Copper mineralization styles within the study area can be classified into basalt-hosted and sediment-hosted.

The first style encompasses native copper ± native silver hosted by flow-top mafic lavas. Native copper typically occurs as infill material within vesicles (Fig. 3A) and, to a lesser extent, in veinlets. It is consistently associated with intense hydrothermal alteration characterized by quartz and green minerals such as epidote, prehnite, and chlorite. Native silver, appearing as wire-shaped crystals, exhibits an erratic distribution. This mineralization is predominantly concordant and exclusive to amygdaloidal basalts. However, in localized places (P1, P2, and P4 in Fig. 1C), minor occurrences of native copper are also found in sulfide-hosting veinlets and hydrothermal breccias, both of which are associated with weakly altered non-vesicular basalts.

The second style includes sediment-hosted Cu-sulfides. Despite the "La Quinta" Formation being dominated by red beds, copper mineralization predominantly occurs in greenish, brownish, and light-gray layers of siltstones, as well as medium- to fine-grained arkoses and sandstones (Fig. 3B). Cu-sulfides manifest in drusiform and banded veinlets, disseminated along bedding planes, and within quartz-rich hydrothermal breccias (Fig. 3C). Layers that are non-red typically exhibit hydrothermal alteration (silicification, Ca-CO_2-rich, and Ca-Si-rich alterations) and contain charcoal. (Fig. 3D). Angular charcoal clasts, ranging from 1 to 5 cm in diameter, are erratically distributed in coarse-grained gray beds (Fig. 3D).

Mineral assemblages

1. Basalt-hosted

Hydrothermal alteration in mafic flow-top lavas is characterized by four distinct stages occurring in chronological order: (i) Na-rich alteration, (ii) K-rich alteration, (iii) Ca-Si-rich alteration, and (iv) Ca-CO_2-rich alteration.

Na-rich alteration is widespread in the basalts and involves crustiform albite veinlets with minor quartz and earthy hematite (Fig. 4A). Plagioclase phenocrysts are often replaced by whitish to slightly pinkish, occasionally coarse albite.

K-rich alteration is observed locally and encompasses pink K-feldspar and quartz traces. K-feldspar veinlets crosscut former albite and are confined to zones of intense brecciation in non-vesicular basalts (Fig. 4B).

The Ca-Si-rich alteration stage is dominated by an assemblage of calcium-bearing minerals, including epidote, prehnite, and minor garnet (Fig. 4C). Quartz, chlorite, specularite, and tourmaline are also prevalent during this stage (Fig. 4D). This alteration is highly pervasive in the vesicular basalts, where original textures have been completely obliterated. Epidote, the most abundant mineral during this stage, occurs in veinlets, filling vesicles and most commonly replacing the volcanic host rock as massive patches. Epidote crystals exhibit various habits, including fan-like shapes, elongated prisms, and fibrous arrangements. In non-vesicular basalts, this mineral is restricted to veinlets with multiple episodes of opening (Fig. 4C). Prehnite is ubiquitous, occurring as fan-shaped crystals intimately associated with epidote and quartz (Fig. 4D). Garnet is scarce and mostly replaced by clinozoisite.

The ore minerals paragenetically associated with Ca-Si-rich alteration vary in vesicular and non-vesicular basalts. Vesicular basalts host exclusively native copper and traces of wire-shaped native silver (Fig. 4E, F), whereas non-vesicular basalts host bornite, covellite, chalcopyrite, undifferentiated Cu-sulfides and euhedral specularite (Fig. 4G, H, I). Mirmekitic intergrown of bornite and digenite are widespread. Besides, most of the sulfides are usually replaced by malachite (Fig. 4B).

Finally, the Ca-CO_2-rich alteration stage encompasses white calcite and minor calcium-rich zeolites occurring as veinlets and infill of open spaces (Fig. 4J, K, L). Calcite often surrounds and replaces albite, quartz, prehnite, and other minerals from previous stages (Fig. 4K).

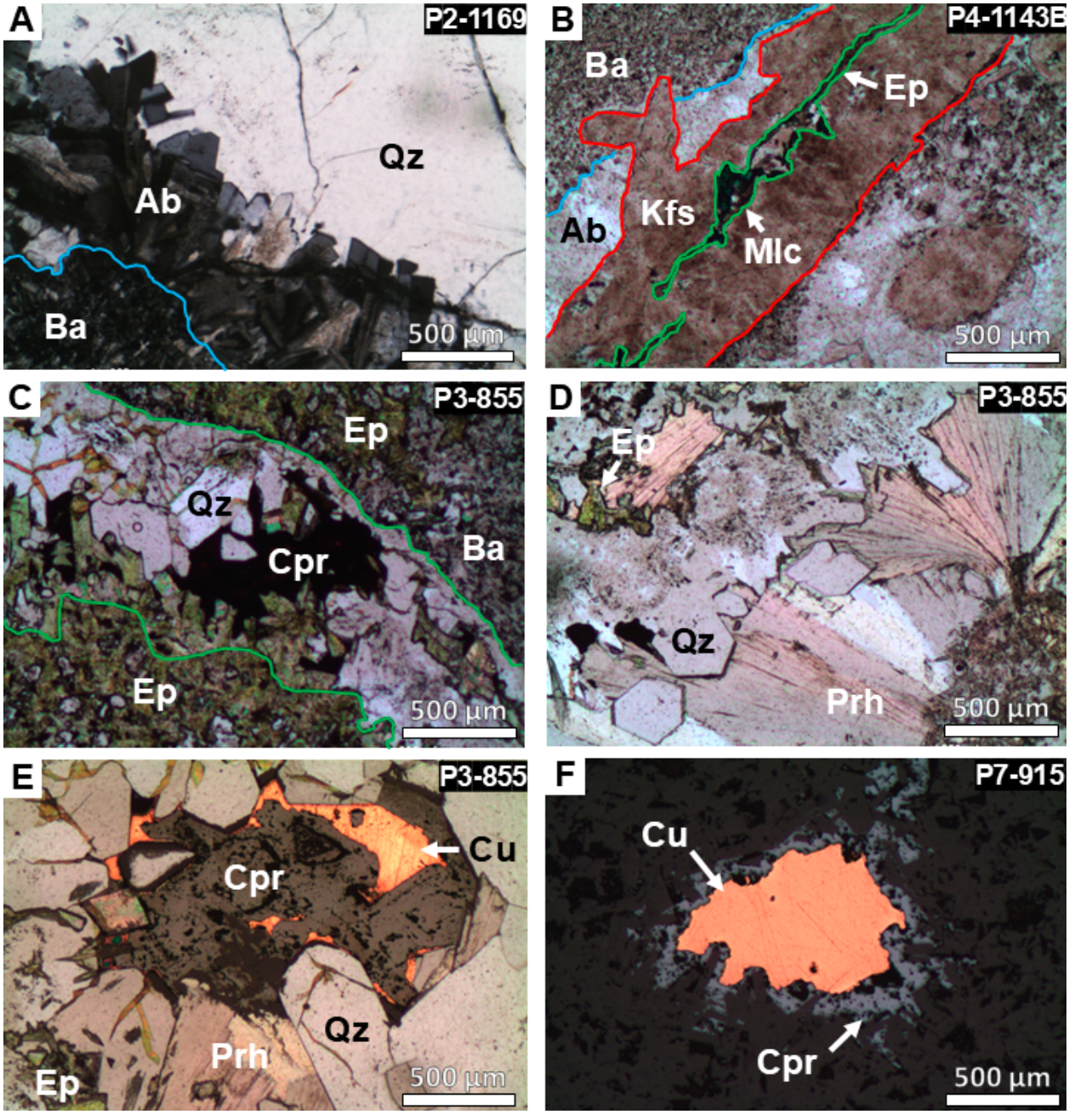

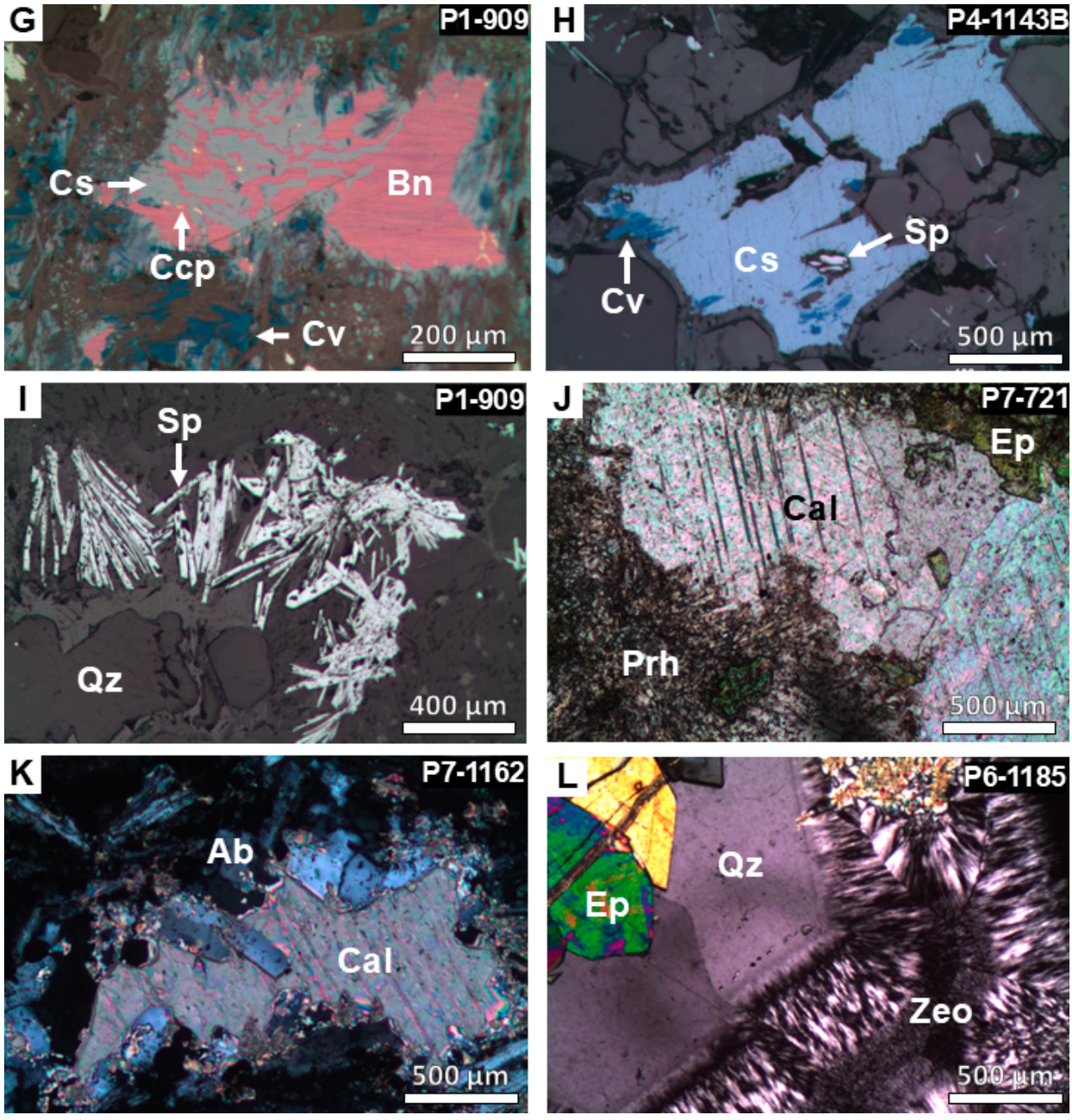

Figure 4. Microphotographs of typical mineral assemblages of basalt-hosted mineralization. **A)** Basalt altered to albite and crosscut by a vein consisting of albite and quartz. **B)** Non-vesicular basalt affected by three alteration stages consisting of albite, k-feldspar, and epidote - malachite. **C)** Pervasive epidotization affecting amygdaloidal basalt. There is also a veinlet composed of quartz, epidote and cuprite after native copper. **D)** Vein containing euhedral quartz, fan-shaped prehnite and epidote. **E)** Amygdule consisting of native copper, cuprite, quartz, prehnite and epidote. **F)** Amygdule only consisting of native copper; Note the cuprite corona around native copper. **G)** Non-vesicular basalt hosting Cu-sulfides, bornite, covellite and chalcopyrite. Note the mirmekitic intergrown between bornite and the Cu-sulfides. **H)** Quartz vein containing covellite, Cu-sulfides and specularite. **I)** Euhedral specularite and quartz. **J)** Calcite veinlet crosscutting epidote and prehnite assemblage. Note calcite surrounds some epidote fragments. **K)** Albite crystals partially replaced by calcite. **L)** Euhedral quartz and epidote with late-stage calcium-rich zeolite. Abbreviations: Ab – Albite, Ba – Basalt, Bn – Bornite, Cal – Calcite, Ccp – Chalcopyrite, Cpr – Cuprite, Cs – Cu-sulfides, Cu – Native Copper, Cv – Covellite, Ep – Epidote, Kfs - K-felspar, Mlc – Malachite, Prh – Prehnite, Qz – quartz, Sp – Specularite, Zeo – Zeolite.

2. Sediment-hosted

Compared to basalt-hosted mineralization, sediment-hosted was only associated with (i) Ca-Si-rich and (ii) Ca-CO_2-rich alteration assemblages.

In sediment-hosted deposits, the Ca-Si-rich alteration is less intense and consists of clinozoisite, chlorite, and abundant quartz veinlets with Cu-sulfides (Fig 5A, B). The primary ore minerals associated with this alteration include bornite, covellite, chalcopyrite, undifferentiated Cu-sulfides, and specularite (Fig. 5C, D, E, F). Bornite and chalcopyrite often display reaction rims of covellite and undifferentiated Cu-sulfides (Fig. 5D). Specularite occurs as euhedral crystals forming intergrowths with sulfides or containing chalcopyrite inclusions (Fig. 5E). Mirmekitic intergrowths of bornite and undifferentiated Cu-sulfides are also observed (Fig. 5F). These replacement rims and interstitial textures of Cu-sulfides were also evidenced through Back-scattered electron (BSE) images (Fig. 6A, C, E). Pyrite is rarely observed, appearing as framboidal and cubic aggregates commonly replaced by bornite, specularite, and undifferentiated Cu-sulfides (Fig. 5G). Moreover, silicification and brecciation are also associated with this alteration.

In specific locations, covellite and other undifferentiated Cu-sulfides related to the Ca-Si-rich alteration were found spatially associated with charcoal clasts consisting of semifusinite. These clasts display well-preserved plant cell wall structures, and their primary porosity is occupied by Cu-sulfides (Fig. 5H). On the other hand, copper mineralization was also associated with tabular and highly fractured fragments of organic matter exhibiting moderate reflectance and strong anisotropy, probably corresponding to pyrobitumen (?) (Fig. 5I). Both semifusinite and pyrobitumen (?) were recognized through BSE images. Pyrobitumen (?) fragments display a dark appearance indicative of a light elemental composition (Fig. 6G) and the plant cell wall structures of semifusinite were observable (Fig. 6H).

Finally, the Ca-CO_2-rich alteration assemblage includes calcite veinlets and breccias crosscuting former quartz and sulfide veins (Fig. 5J).

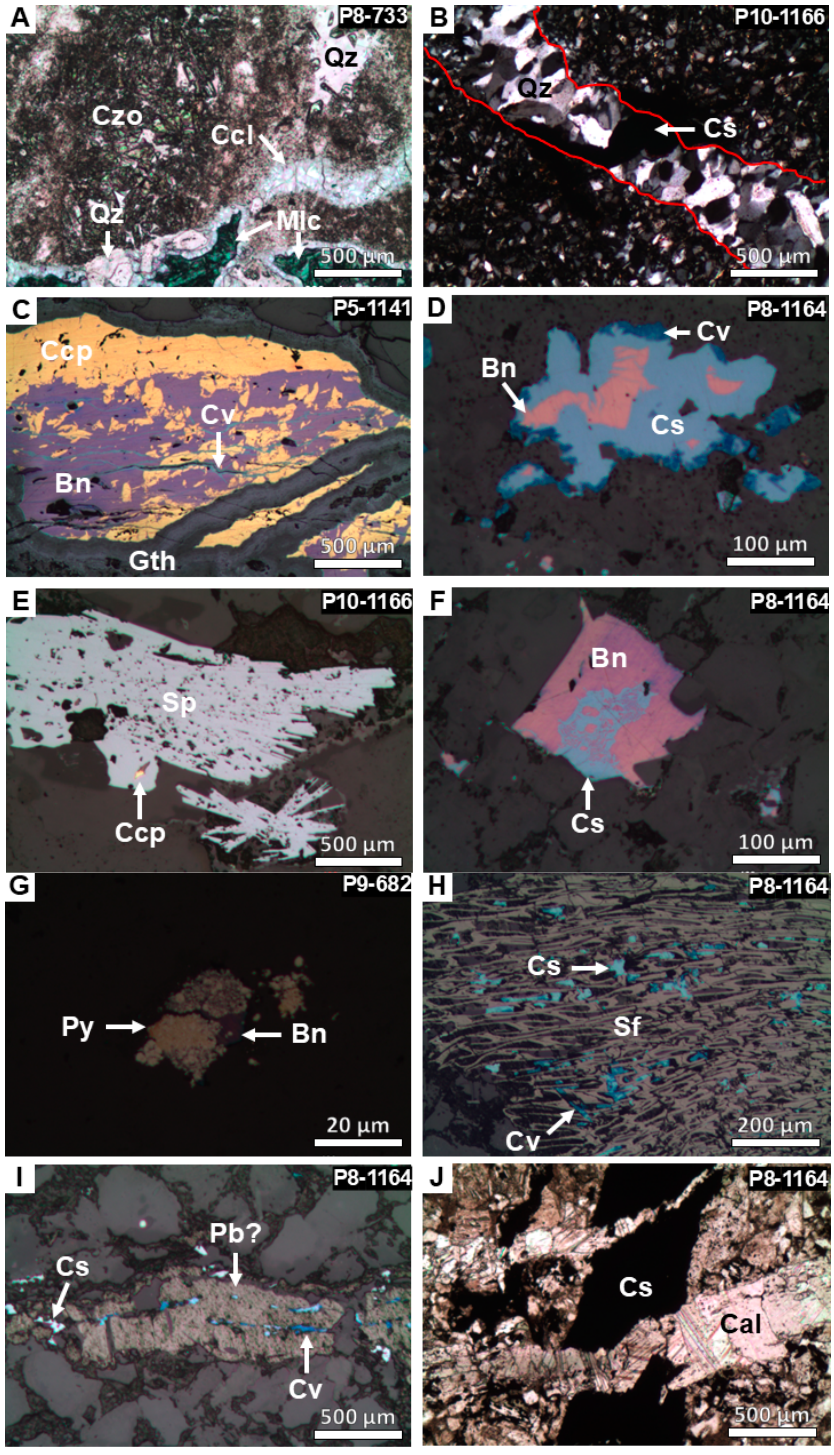

Figure 5. Microphotographs of sediment-hosted mineralization. **A)** Gray siltstone hosting clinozoisite and quartz associated with malachite (Ma) and chrysocolla after Cu-sulfides. **B)** Arkosic sandstone crosscut by a veinlet consisting of quartz and Cu-sulfides. **C)** Chalcopyrite and bornite vein; Covellite and goethite are observed filling fractures. **D)** Bornite, covellite and Cu-sulfides assemblage. **E)** Euhedral specularite exhibiting a chalcopyrite inclusion. **F)** Mirmekitic intergrowth of bornite and Cu-sulfides. **G)** Aggregates of framboidal pyrite partially replaced by bornite. **H)** Charcoal fragment made up of semifusinite spatially associated with covellite and Cu-sulfides. **I)** Pyrobitumen (?) fragment associated with covellite and Cu-sulfides. **J)** Calcite veinlets crosscutting Cu-sulfides (Cs). Abbreviations: Bn – Bornite, Cal – Calcite, Ccp – Chalcopyrite, Chr – Chrysocolla, Cs – undifferentiated Cu-sulfides, Cv – Covellite, Czo – Clinozoisite, Gth – Goethite, Mlc – Malachite, Pb? - Pyrobitumen (?), Py – Pyrite, Qz – Quartz, Sf – Semifusinite, Sp – Specularite.

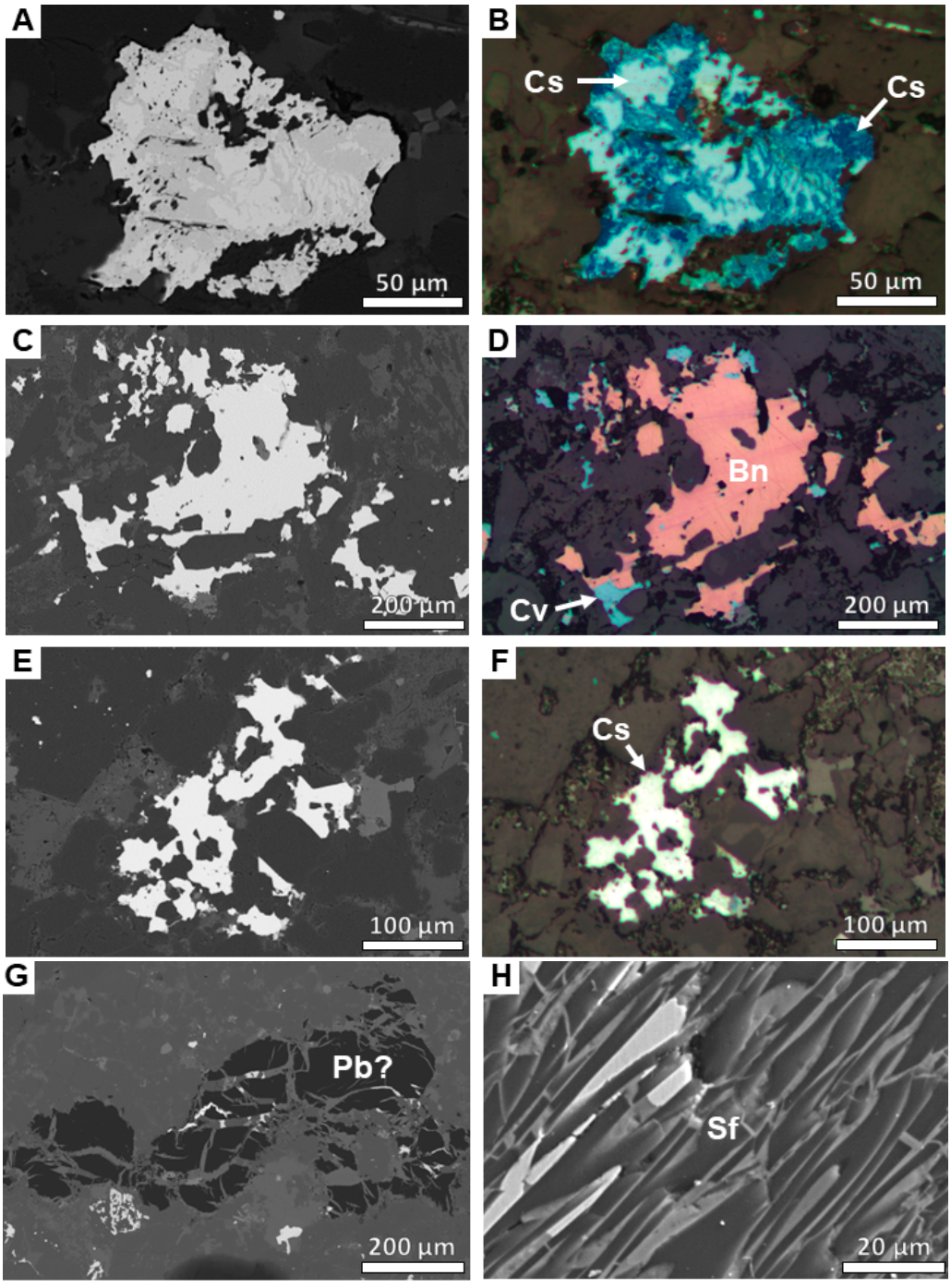

Figure 6. Backscattered electron (BSE) images of Cu-sulfides and organic compounds from the "La Quinta" Formation. Reflected polarized light (PPR) microphotographs of the Cu-sulfides were included for comparison. **A)** and **B)** Cu-sulfides showing replacement texture. **C)** and **D)** Bornite exhibiting covellite rim. **E)** and **F)** Interstitial Cu-sulfides grains. **G)** Highly fractured pyrobitumen (?) fragment. Its dark color indicates a light elemental composition. **H)** Well-preserved plant cell structures (i.e. semifusinite). Abbreviations: Bn – Bornite, Cs – undifferentiated Cu-sulfides, Cv – Covellite, Pb? – Pyrobitumen (?), Sf – Semifusinite.

3. Supergene environment

In vesicular basalts, supergene oxidation of native copper has formed Cu-oxides such as cuprite and minor tenorite, delaffosite, and paramelaconite (Fig.7A, B, C). Cuprite typically occurs along fractures and forms rims around native copper crystals (Fig. 4E, F; Fig. 7A). Cu-carbonates (i.e. malachite and azurite) are also commonly found filling fractures and replacing native copper and Cu-sulfides (Fig. 7C, D). Conversely, epidote and prehnite remain unaffected by supergene oxidation.

Contrastingly, the oxidation process of the sediment-hosted sulfides generates goethite, covellite, chrysocolla, malachite, and azurite. As sulfide-rich veins oxidize, banded aggregates of botryoidal goethite and radial malachite and chrysocolla form (Fig. 5A, C; Fig. 7E, F). Malachite often replaces calcite, whereas chrysocolla forms reaction rims around quartz (Fig. 7F). Besides, specularite is usually unaffected by weathering, coexisting with malachite and azurite.

As a summary of the identified mineral assemblages, Fig. 8 shows the paragenetic sequence for mineralization.

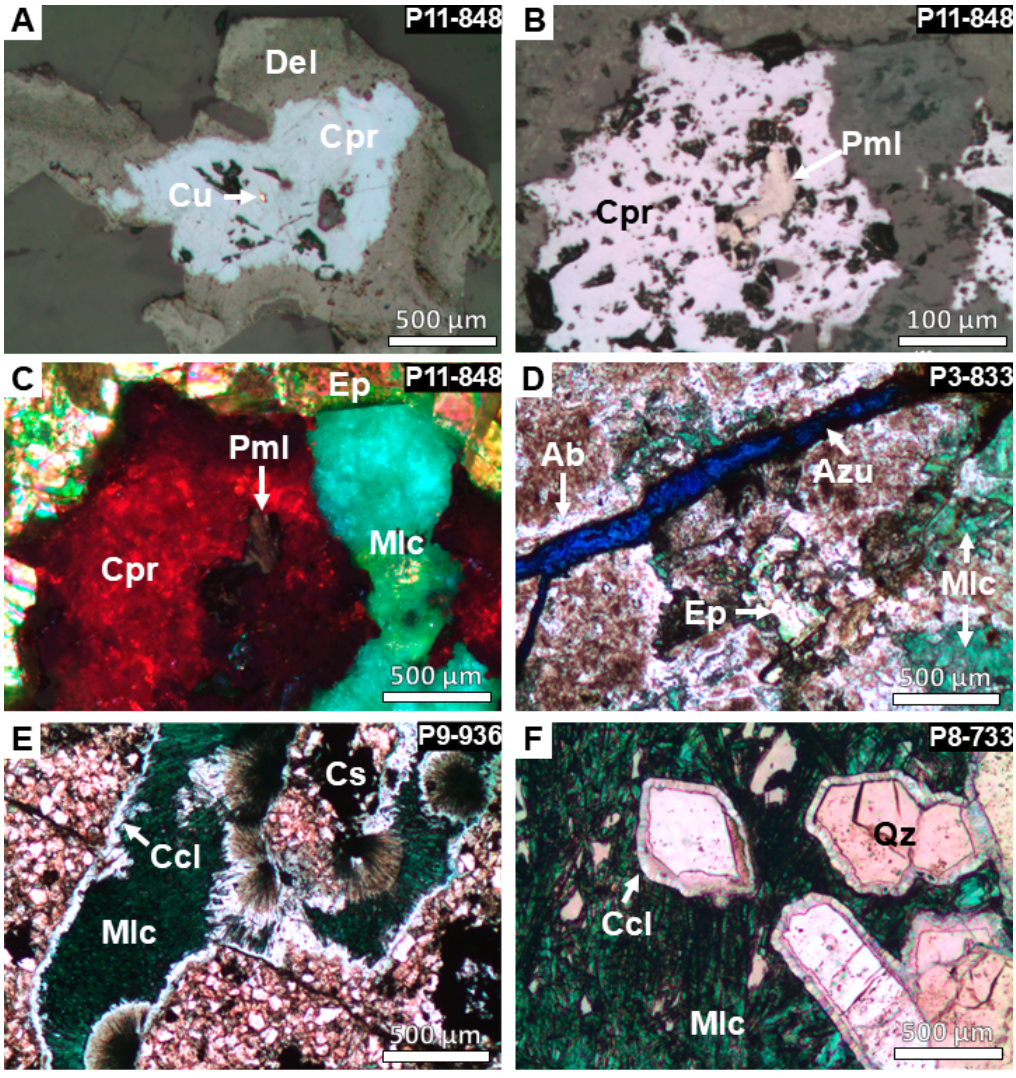

Figure 7. Microphotographs of supergene mineral assemblages for basalt-hosted (A-D) and sediment-hosted (E-F) mineralization. **A)** Minute relic of native copper surrounded by cuprite and delaffosite corona. **B)** Cuprite and paramelaconite assemblage after native copper. **C)** Cuprite, paramelaconite, malachite and epidote assemblage. **D)** Azurite and malachite filling fractures in a basalt altered to albite and epidote. **E)** Sandstone containing banded veinlets of radial malachite and chrysocolla. Note there are some relics of Cu-sulfides. **F)** Siltstone hosting malachite and chrysocolla. Note chrysocolla forms reaction rims that partially replace quartz. Abbreviations: Ab – Albite, Azu – Azurite, Ccl – Chrysocolla, Cpr – Cuprite, Cu – Native Copper, Del – Delafossite, Ep – Epidote, Mlc – Malachite, Pml – Paramelaconite, Qz – Quartz.

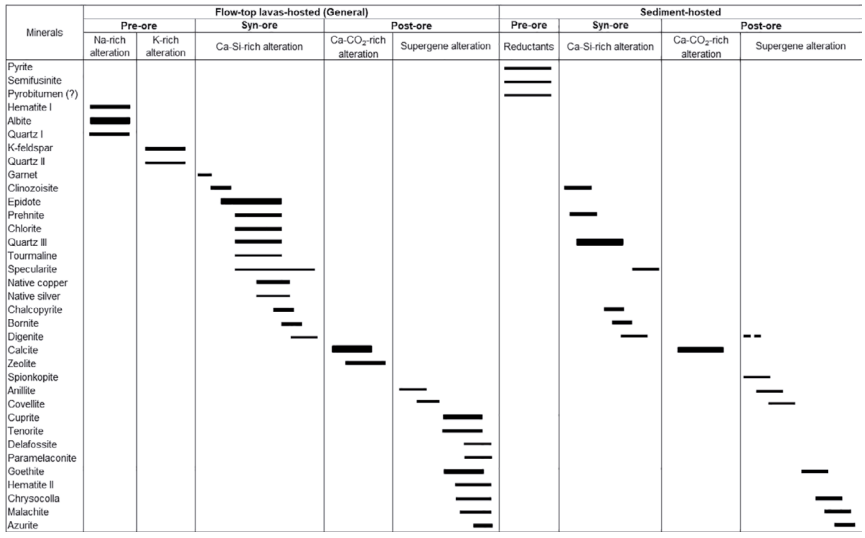

Figure 8. Schematic paragenetic sequence for basalt- and sediment-hosted Cu (±Ag) mineralization in the "La Quinta" Formation. Anilite, spionkopite and digenite (undifferentiated Cu-sulfides in this chapter) were added based on mineral chemistry results.

Mineral Chemistry

Electron Probe Micro-Analyzer (EPMA) analyses enabled the detailed mineral composition assessment of Cu-sulfides, Cu-Fe-sulfides, native copper, and pyrite as displayed in Table 1.

The chemical composition of Cu-sulfides and Cu-Fe-sulfides varies across the different detected elements. The S content ranges from 21.06 to 32.78 wt% in Cu-sulfides, while in Cu-Fe-sulfides it spans from 26.32 to 35.53 wt%. The Cu concentration in Cu-sulfides varies from 67.48 to 78.90 wt%, whereas in Cu-Fe sulfides it ranges from 33.71 to 62.55 wt%. The Fe content for Cu-sulfides ranges from <0.001 up to 3.87 wt%, while Cu-Fe-sulfides exhibit concentrations from 10.95 to 30.91 wt%. Lastly, Ag content varies between <0.003 and 0.13 wt% in Cu-sulfides, whereas in Cu-Fe-sulfides it is slightly higher, ranging from 0.04 to 0.31 wt%.

Besides, the analyzed Cu-sulfides exhibit a composition range from $Cu_{1.04}S$ to $Cu_{1.089}S$. The prior allows the differentiation between anilite, covellite, digenite, and spionkopite. Anilite has an average composition of $Cu_{1.74}S$, covellite of $Cu_{1.04}S$, digenite of $Cu_{1.86}S$, and spionkopite is characterized by $Cu_{1.38}S$. Additionally, the Cu-Fe-sulfides (i.e. chalcopyrite and bornite) have average compositions of $Cu_{0.99}Fe_{1.01}S_2$ and $Cu_{4.52}Fe_{1.06}S_4$, respectively.

As depicted in Fig. 9, the metal/sulfur ratio ([Cu + Fe + Ag]/S) indicates that bornite, chalcopyrite, digenite, and the unidentified Cu-sulfide are the main Ag host minerals. The plot also displays a wide range of variation in the (Cu + Fe + Ag)/S and Cu/S ratios. The former spans from 1.5 to 4, and the latter varies from 0.95 to 3.75.

On the other hand, the analyzed native copper crystals have an average Cu content of 97.67 wt% and show traces of S (average: 0.256 wt%), Fe (average: 0.039 wt%) and Ag (average: 0.027 wt%). An anomalous Ag-rich native copper crystal yielded average Cu and Ag contents of 62.58 wt% and 31.39 wt%, respectively.

Lastly, pyrite crystals have an average S composition of 51.93 wt% and an average Fe content of 46.62 wt%. Besides, Cu and Ag were also identified in pyrite, ranging from <0.005 to 0.98 wt% for the former and <0.004 to 0.031 wt% for the latter.

Table 1. Representative EPMA analyses of selected ore minerals from the "La Quinta" Formation (in wt.%). bdl: below detection limit.

Mineral	S	Cu	Fe	Ag	Total	Cu/S	Formula	Sample
Anilite	22.50	77.97	0.001	0.003	100.47	3.47	$Cu_{1.75}S$	1164-P8
Anilite	22.69	77.67	bdl	0.012	100.37	3.42	$Cu_{1.72}S$	1164-P8
Covellite	32.78	67.48	0.35	0.03	100.64	2.06	$Cu_{1.04}S$	1164-P8
Covellite	32.57	67.75	0.04	0.06	100.42	2.08	$Cu_{1.05}S$	1164-P8
Digenite	21.06	78.90	0.18	0.04	100.18	3.75	$Cu_{1.89}S$	1164-P8
Digenite	21.58	77.85	0.04	0.12	99.59	3.61	$Cu_{1.82}S$	938-P1
Spionkopite	27.66	72.49	0.02	0.08	100.25	2.62	$Cu_{1.32}S$	1164-P8
Spionkopite	25.32	72.94	1.32	bdl	99.57	2.88	$Cu_{1.45}S$	1143B-P4
Cu-sulfide	22.41	72.83	3.87	0.13	99.24	3.25	$Cu_{1.64}Fe_{0.09}S$	1141-P5
Bornite	27.67	53.47	16.54	0.04	97.72	1.93	$Cu_{3.90}Fe_{1.37}S_4$	1164-P8
Bornite	26.54	61.82	11.37	0.31	100.04	2.33	$Cu_{4.70}Fe_{0.98}S_4$	1141-P5
Bornite	26.32	62.41	11.13	0.09	99.94	2.37	$Cu_{4.78}Fe_{0.97}S_4$	1141-P5
Bornite	26.71	62.55	10.95	0.09	100.31	2.34	$Cu_{4.72}Fe_{0.94}S_4$	938-P1
Chalcopyrite	34.91	34.91	29.36	0.11	99.30	1.00	$Cu_{1.01}Fe_{0.96}S_2$	1141-P5
Chalcopyrite	35.53	33.71	30.30	bdl	99.54	0.95	$Cu_{0.96}Fe_{0.98}S_2$	1141-P5
Chalcopyrite	35.03	34.53	30.75	0.06	100.37	0.99	$Cu_{0.99}Fe_{1.01}S_2$	1197-P9
Chalcopyrite	34.33	34.08	30.752	0.104	99.275	0.99	$Cu_{1.00}Fe_{1.03}S_2$	1197-P9
Chalcopyrite	34.97	34.36	30.68	0.06	100.08	0.98	$Cu_{0.99}Fe_{1.01}S_2$	1197-P9
Chalcopyrite	34.96	34.32	30.91	0.07	100.28	0.98	$Cu_{0.99}Fe_{1.01}S_2$	1197-P9
Native copper	0.09	99.96	bdl	0.02	100.07	-	$Cu_{99.89}Ag_{0.02}$	1143-P4
Native copper	0.09	99.08	bdl	0.01	99.18	-	$Cu_{99.90}Ag_{0.01}$	1143-P4
Native copper	bdl	98.75	bdl	0.043	98.793	-	$Cu_{99.96}Ag_{0.04}$	848-P11
Native copper	0.145	99.062	0.012	0.018	99.237	-	$Cu_{99.82}Ag_{0.02}$	1045-P6
Native copper	0.524	93.977	0.071	0.032	94.604	-	$Cu_{99.34}Ag_{0.03}$	1045-P6
Native copper	0.432	62.579	0.015	31.39	94.412	-	$Cu_{66.28}Ag_{33.24}$	2-P7
Native copper	bdl	95.209	0.058	0.043	95.31	-	$Cu_{99.89}Ag_{0.05}$	2-P7
Pyrite	49.01	0.98	46.50	bdl	96.49	-	$Fe_{1.09}S_2$	1143B-P4
Pyrite	52.442	0.008	46.95	0.031	99.431	-	$Fe_{1.03}S_2$	968-P9
Pyrite	52.402	0.005	46.79	bdl	99.197	-	$Fe_{1.02}S_2$	968-P9
Pyrite	52.114	bdl	46.445	0.004	98.563	-	$Fe_{1.02}S_2$	969-P9
Pyrite	52.12	bdl	46.397	0.012	98.529	-	$Fe_{1.02}S_2$	969-P9
Pyrite	52.327	0.013	46.305	0.015	98.66	-	$Fe_{1.01}S_2$	969-P9
Pyrite	53.068	0.019	46.93	0.022	100.039	-	$Fe_{1.01}S_2$	970-P9

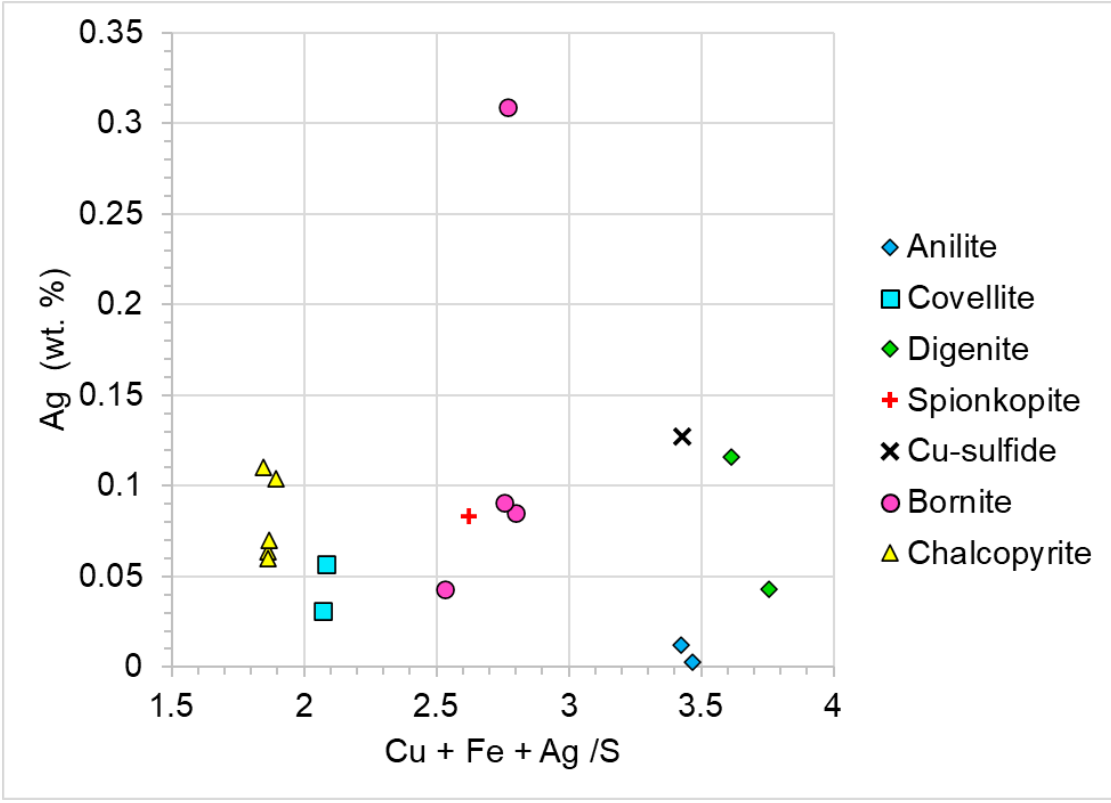

Figure 9. EPMA data for Cu-sulfides and Cu-Fe-sulfides plotted as Ag (wt.%) vs. [Cu + Fe + Ag] / S, showing that the highest silver concentrations (> 0.1 wt. %) are associated with bornite, chalcopyrite, digenite and unidentified Cu-sulfide.

Lithogeochemistry

Table 2 presents the chemical composition of five outcrop rock samples with different degrees of alteration and mineralization. The samples include a Cu-rich vesicular basalt with intense Ca-Si-rich alteration characterized by abundant epidote (1161-P7), a basalt with moderate epidotization (i.e. Ca-Si-rich alteration) (1225-P4), a basalt affected by Ca-CO_2-rich alteration (1163-P7), a Cu-rich sandstone (1164-P8), and an unaltered siltstone (1233-P8).

Fig. 10 displays mass balance diagrams illustrating the main changes in elemental composition after hydrothermal alteration. The composition of basalt samples (1161-P7, 1225-P4, and 1163-P7) was normalized using the compositional values of sample 1125 (unaltered basalt) from Cano et al. (2022). In contrast, the mineralized sandstone composition (1164-P8) was normalized with data from sample 1233-P8 (unaltered siltstone).

Major elements in the intensely epidotized basalt (1161-P7) evidence an increase in Fe_2O_3, CaO, Cr_2O_3, TiO_2, MnO, and SrO contents, while depletion of MgO, Na_2O, K_2O is observed (Fig. 10A). Trace elements behavior shows an addition of Ga and V, while Cs, Rb, Co, Li, Ni, and Zn are diminished (Fig. 10C). In contrast, both major and trace elements do not vary significantly in the moderately epidotized basalt (1225-P4) (Fig. 10 A, C). Besides, the basalt affected by Ca-CO_2-rich alteration (1163-P7) shows enrichment in CaO, K_2O, Cr_2O_3, and TiO_2, while Al_2O_3, MgO, and SrO are depleted (Fig. 10A). For this sample, contents of trace elements such as Cs, Rb, As, and Ni increase unlike Ga, Th, U, V and Li which are reduced (Fig. 10C). On the other hand, the Cu-rich sandstone (1164-P8) exhibits an increase in the concentration of CaO, Na_2O, TiO_2, MnO, and P_2O_5 along with depletion of K_2O, and BaO (Fig. 10B). This sample evidence alteration in terms of Sr, U, Zr, Nb and Ta, while contents of Cs, Rb W, Sc, Ni, Pb, and Zn show depletion (Fig. 10D).

Additionally, hydrothermal alteration influences the variation of large-ion lithophile elements (LILEs). The basalt sample with intense Ca-Si-rich alteration (1161-P1) and the Cu-rich sandstone (1164-P8) show strong depletion on LILEs such as K, Rb, and Cs. Oppositely, there is enrichment of the same elements in the basalt with Ca-CO_2-rich alteration (1163-P7) (Fig.A, B, C, D).

Furthermore, there is no significant alteration of SiO_2 in the basalts affected by Ca-Si-rich and Ca-CO_2-rich alterations, nor in the Cu-rich sandstone (Fig. 10A, B). Likewise, the behavior of Rare Earth Elements (REE) in both analyzed lithologies shows no significant variation, implying no REE mobility (Fig. 10E, F).

Discussion

Hypogene versus supergene mineralization

Field and mineralogical observations of basalt-hosted native copper and native silver support their hypogene, epigenetic origin, in association with minerals such as epidote, prehnite, chlorite, and quartz (Fig 9). Additionally, we identified cuprite, tenorite, delafossite, paramelaconite, malachite, and azurite as products of in-situ supergene oxidation, replacing the native copper.

The sediment-hosted copper mineralization includes primary/hypogene chalcopyrite, bornite and digenite. EPMA results revealed the presence of sulfides of the Cu-S system (digenite-chalcocite series), specifically covellite, anilite, spionkopite, and digenite. Spionkopite and anilite mainly occur in Cu-bearing deposits, and their formation is interpreted as a low-temperature transformation of hypogene sulfides (Hatert, 2005; Gablina et al., 2004; Sadati et al., 2016). The scarcity of chalcocite might indicate its complete transformation into spionkopite and anilite, which are more stable under low-temperature conditions (Gablina et al., 2004). Therefore, the mineral assemblage has been interpreted as digenite + anilite + spionkopite + covellite, occurring in sediment-hosted and basalt-hosted styles in the “La Quinta” Formation. Subsequent weathering of sediment-hosted Cu-rich sulfides caused their replacement by malachite, azurite, chrysocolla, and goethite. It is noteworthy that digenite occurs in both stages: i) associated with hypogene bornite, as symplectitic texture coexistence (Fig. 6F) and (ii) as part of the supergene mineral assemblage (Fig.7B, C).

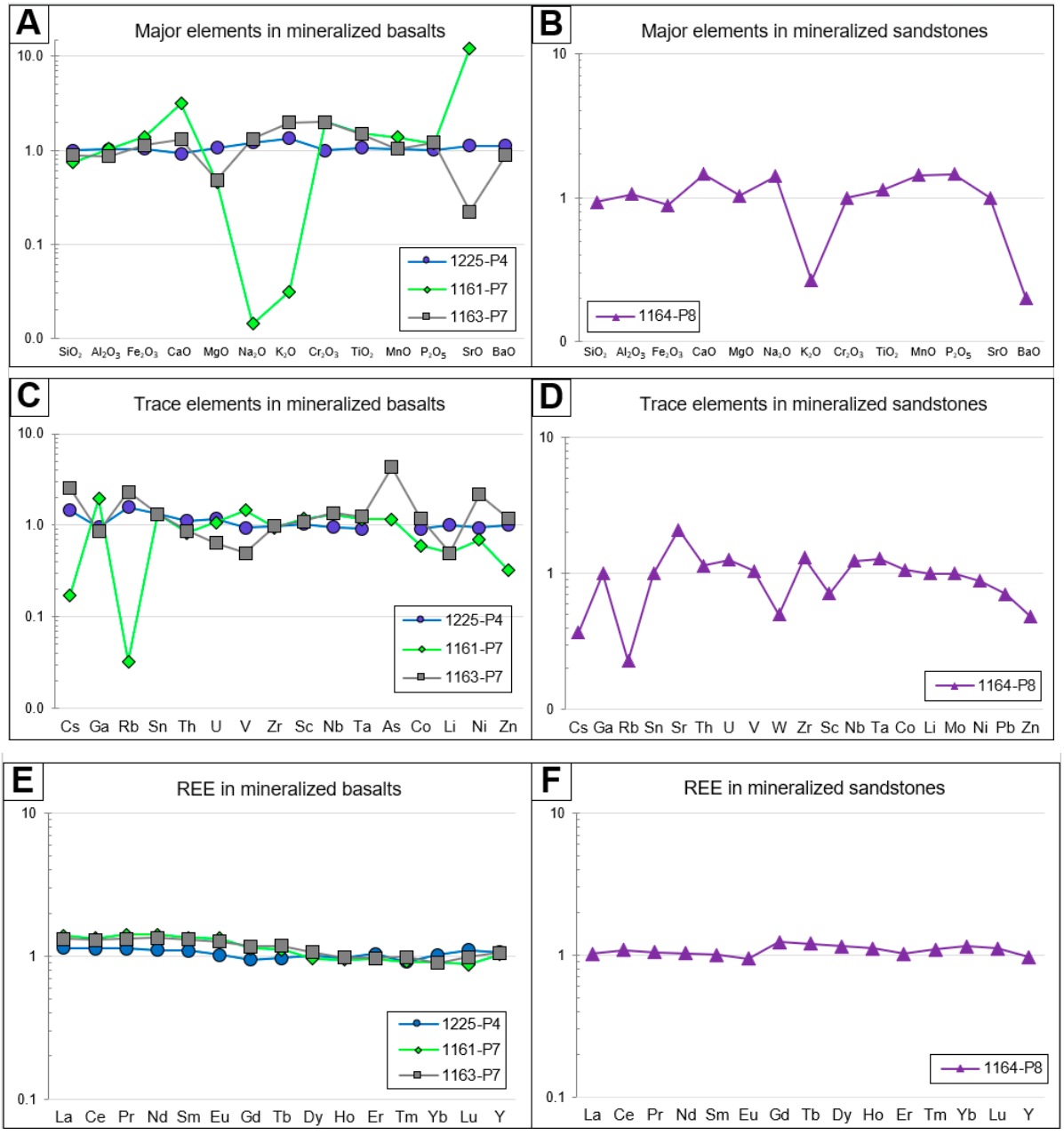

Figure 10. Multielement diagrams showing the normalized distribution of major, trace, and rare earth elements (REE). Basalt samples were normalized with respect to sample 1125 (unaltered basalt) described by Cano et al. (2022), while the sandstone sample was normalized using sample 1233-P8 (unaltered siltstone). A)-B) Major elements in mineralized basalts and sandstone. C)-D) Trace elements variation in mineralized basalts and sandstone. E)-F) REE distribution in mineralized basalts and sandstone.

Table 2. Chemical composition of selected rock samples. HEB: Basalt with intense Ca-Si-rich alteration; MS: Mineralized sandstone; CB: Basalt with Ca-CO_2-rich alteration; NS: unmineralized siltstone; MEB: Basalt with moderate Ca-Si-rich alteration; LOI: loss on ignition.

Sample	1161-P7	1164-P8	1163-P7	1233-P8	1225-P4		1161-P7	1164-P8	113-P7	1233-P8	1225-P4
Lithology	HEB	MS	CB	NS	MEB	Sc	17	10	16	14	15
Major elements (wt. %)						La	42.2	19.8	40.1	19.4	34.6
SiO_2	41	66.5	49	71.1	54.8	Ce	86.2	38.5	84.1	35.5	73.2
Al_2O_3	17.3	10.75	14.35	10.15	17	Pr	10.9	5.16	10.2	4.95	8.69
Fe_2O_3	12.1	4.44	9.8	5	9	Nd	43.7	21	41.4	20.5	33.9
CaO	20.4	3.42	8.42	2.34	5.93	Sm	8.36	4.51	8.2	4.5	6.82
MgO	1.78	2.66	1.88	2.59	4.13	Eu	2.47	0.93	2.36	0.99	1.9
Na_2O	0.05	3.22	4.67	2.29	4.26	Gd	7.15	4.53	7.39	3.67	5.95

Sample	1161-P7	1164-P8	1163-P7	1233-P8	1225-P4		1161-P7	1164-P8	113-P7	1233-P8	1225-P4
K_2O	0.04	0.59	2.53	2.22	1.72	Tb	1	0.65	1.06	0.54	0.87
Cr_2O_3	0.02	0.01	0.02	0.01	0.01	Dy	5.1	4.05	5.62	3.52	5.36
TiO_2	1.86	1.04	1.84	0.92	1.32	Ho	0.97	0.81	1	0.73	1
MnO	0.2	0.1	0.15	0.07	0.15	Er	2.65	2.31	2.66	2.27	2.85
P_2O_5	0.58	0.16	0.6	0.11	0.5	Tm	0.36	0.36	0.39	0.33	0.36
SrO	0.55	0.02	0.01	<0.01	0.05	Yb	2.22	2.47	2.2	2.15	2.49
BaO	<0.01	0.01	0.04	0.05	0.05	Lu	0.31	0.39	0.35	0.35	0.39
LOI	3.42	5.21	7.43	3.71	2.6	Hf	6.5	12.2	5.7	8.1	5.5
Total	**99.3**	**98.1**	**100.7**	**100.6**	**101.5**	**Y**	**27.7**	**24.1**	**28.5**	**25**	**28.7**
Trace elements (ppm)						Nb	25.9	13.2	27	10.7	18.9
Ba	9.9	135.5	394	448	457	Ta	1.4	0.9	1.5	0.7	1.1
Cr	150	80	150	100	50	Ag	5.1	12.5	<0.5	<0.5	<0.5
Cs	0.05	0.63	0.74	1.71	0.42	As	7	<5	26	7	<5
Ga	42.1	13.3	18.6	13.3	20.5	Cd	<0.5	<0.5	<0.5	<0.5	<0.5
Rb	1	20.6	71.1	90.6	48.6	Co	15	16	30	15	23
Sn	2	2	2	2	2	Li	10	40	10	40	20
Sr	4550	174	130.5	83.2	398	Mo	1	1	<1	1	1
Th	3.89	5.97	4.11	5.21	5.32	Ni	32	22	99	25	43
U	1.04	1.87	0.62	1.49	1.13	Pb	36	12	32	17	<2
V	262	175	90	168	169	Tl	<10	<10	<10	10	<10
W	<1	1	2	2	<1	Zn	35	63	129	130	109
Zr	262	461	270	353	270	Cu	13600	13500	29	33	122

In the "La Quinta" Formation, the development of a supergene enrichment blanket involving leaching and a secondary accumulation of copper is improbable. First, the lack of pyrite in the host rocks and favorable alteration mineralogy prevents the formation of sulfuric acid from weathering. Second, the widespread occurrence of acid-neutralizing minerals, such as carbonates, feldspars, and silicates, precludes the acidification of oxidizing solutions. Consequently, supergene oxidation of the Cu ores in the "La Quinta" Formation has only led to the formation of in-situ minerals stable under near neutral pH (Chavez, 1990).

Ore forming conditions

Based on mineral stability ranges and microthermometry studies of fluid inclusions in gangue minerals, González-Duran (2016) indicated that hypogene mineralization occurred at 100-260°C, caused by the circulation of moderately saline and highly oxidized fluids with near neutral pH. Their estimates align with the mineral assemblages observed in this study. For instance, the minimum crystallization temperature for the albite-K-feldspar alteration assemblages was no less than 150°C (Henley et al., 1983). During calc-silicate alteration, the minimum temperature is well constrained by the appearance of garnet, epidote, and prehnite, spanning 177-200°C (Henley et al., 1983; Bird, 1984; Easton, 1977). The widespread presence of hematite, epidote, calcite, and albite serves as evidence for the saline and oxidized nature of the hydrothermal fluids. Under these conditions, copper and silver are efficiently transported by hydrothermal fluids through complexation with chloride ions (Brown, 2014). For copper to precipitate, abrupt changes in the chemical or physical properties of the aqueous solutions are needed.

In the sediment-hosted ores, the close spatial association of carbonaceous fragments (semifusinite and pyrobitumen?) with Cu-sulfides strongly suggests a genetic link. Organic matter has been shown to be an effective agent for precipitating Cu-sulfides via fluid reduction in stratabound deposits (Wilson and Zentilli, 1999; 2006; Hayes et al., 2015; Herazo et al., 2020; Mahdavi & Rajabi, 2023). Additionally, organic matter may provide reduced sulfur, promoting metal precipitation (Brown, 2014; Herazo et al., 2020). Thus, we propose copper precipitation could have been triggered by organic matter in the charcoal-bearing layers of the La Quinta Formation. The presence of framboidal pyrite in the gray siltstones might have acted as a geochemical trap for copper-bearing fluids to precipitate via replacement of pyrite; this mechanism has been extensively documented in sediment-hosted deposits worldwide (Brown, 2014; Herazo et al., 2020).

On the other hand, the mechanism of native copper +/- silver precipitation in the volcanic rocks should have followed a different pathway since no organic matter is observed in this lithology. Alternative processes may include cooling by mixing with meteoric fluids, reduction of evolved fluids induced by fluid-rock reactions, and copper supersaturation of residual fluids under metamorphic conditions (Jolly, 1974; Brown, 2006; Pinto et al., 2010). For the native copper mineralization style, a sulfur-poor fluid can be inferred based on the lack of sulfur-bearing minerals. Vesicular basalts generally lack volatiles (e.g. sulfur) due to degassing. In contrast, non-vesicular basalts usually contain traces of sulfides (Brown, 2014). For instance, Cano (2015) reports chalcopyrite and bornite inclusions in pyroxenes from non-vesicular basalts from the La Quinta Formation. As proposed by Kirkham (1984), Brown (2014), and Ikehata et al. (2016), hydrothermal fluids can precipitate copper and associated metals by encountering and replacing sulfides. Similarly, in the sediment-hosted domain, pre-ore sulfides such as framboidal pyrite can act as reduced sulfur sources that induce copper precipitation (Brown, 2014; Hayes et al., 2015). Although the aforementioned factors may shed light on copper precipitation, the source of fluids, reduced sulfur, and metals remains uncertain.

Geochemical data shows that the main elements involved in metasomatism are Ca, Mg, Na, K, and Fe. When comparing data from basalts and sediments, there is a consistent trend involving considerable Ca-Mn increase and K-Cs-Rb-Zn depletion. However, the variation of other elements differs. Besides, the element distribution is not uniform in the basalts, reflecting the complexity of hydrothermal alteration overprint at different degrees. These variations are interpreted because of rock-controlled metasomatism, where a similar mineralizing fluid interacts with distinct lithologies, but the mineral and geochemical output may differ according to rock chemistry.

Given that the observations raised in this study are based on a limited number of samples, more data is needed to establish suitable geochemical fingerprints for exploration purposes.

Deposit / District	Commodities	Location	Host rock	Host rock age	Mineralization geochronology	Mineralization Paragenesis	Alteration assamblages	Formation temperatures	Reductants	References
Serrania del Perijá	Cu-(Ag)	Northern Colombia, Eastern Cordillera	Tuffs, rhyolite, andesite, flow-top basalt, siltstone and sandstone.	Jurassic (191 - 164 Ma)	unknown	Cc±Bn±Cu±Ag; Ccp-Bn-Dg-Spi-Ani-Cv; Azu-Mlc-Ccl	Ab-Qz; Kfs-Qz; Ep-Qz-Prh±Chl±Czo±Grt ±Pmp; Cal±Zeo	100 - 260 °C	Semifusinite, pyrite, pyrobitumen (?), and plagioclase. Locally amphibole	González-Durán (2016) Jimenez (2010) Maze (1984) R.P Shawn et al. (2019)
Keshtmahaki	Cu-(Ag)	Southern Iran	Lithic tuffs	Lower Cretaceous	unknown	Cc-Bn-Cu-Ccp±Dg±Cv±Cth	Ep-Chl-Cal-Ser-Qz; Qz-Cal-Ep-Chl-Ab-Hem-Zeo	129 - 145 °C	Pyrite, host rock.	Movahednia et al. (2022) Jiba et al. (2021) Konari et a. (2013)
Cretaceous Cu Belt	Cu-(Ag)	Central Chile	Dacite, andesite, basalt, volcanoclastic units, breccias, conglomerate, limestone.	Lower Cretaceous	90 - 103 Ma	Ccp-Bn±Cc±Dg±Cv±Ttr-Tnt	Ab; Ep-Cal-Chl-Ser-Act-Qz; Bt-Kfs±Tur	150 - 360 °C	Solid bitumen, pyrobitumen, petroleum, framboydal pyrite.	Maureira et al. (2023) Herazo et al. (2020) Kojima et al. (2009) Ramírez et al. (2006)
Jurassic Cu Belt	Cu-(Ag)	Northern Chile	Rhyolite, andesite, basalt.	Upper Jurassic	139 - 168 Ma	Cc-Bn-Dg-Cv±Ccp±Gn; Ata-Ccl			Pyrobitumen	
Kupferschiefer	Cu-Pb-Zn-(Ag)	Poland, Germany	Shale, limestone, evaporites, sandstone, conglomerate.	Permian	53 and/or 149 Ma	Cc-Dg-Bn-Ccp-Cv-Gn-Sp	Hem-Gth (Rote Fäule)	145 - 200°C	Degraded organic matter in shales, pyrite, and possibly methane.	Borg et al. (2012) Hitzman (2010) Hitzman et al. (2005) Vaughan (1989)
Central African Copperbelt	Cu-Co-Ag; Cu-U-Mo-(Au)	Democratic Republic of Congo, Zambia	Shale, siltstone, sandstone.	Neoproterozoic (790 - 840 Ma)	500 - 815 Ma	Cc-Bn-Ccp-Py-Cli; Ccp-Bn-Urn-Bnr-Mol	Kfs-Phl-Ms±Ser; Ser; Ab-Scp; Phl-Anh-Cal-Dol	105 - 400 °C	Hydrocarbons, sour gas, in situ organic matter.	Hitzman (2010) Hitzman et al. (2005) Selley et al. (2005)
Keweenaw Penisula Native Cu Lodes	Cu	Michigan, USA	Basalt, interflow conglomerates.	Mesoproterozoic	1047 - 1060 ± 20 Ma	Cu	Ab-Prh-Lmt-Chl±Anl±Ttn; Ab-Pmp-Prh-Qz-Chl-Ttn±Ep; Ab-Ep-Qz-Chl-Ttn±Pmp	180 - 280 °C	Reductants are not a key factor for ore precipitation (metamorphogenic model).	Brown (2006) Bornhorst et al. (1988) Kirkham (1984) Jolly (1974)
White Pine	Cu-(Ag)	Michigan, USA	Shales, siltstone, Conglomerate, sanstones	Upper Mesoproterozoic (1.078 - 1.085 Ga)	1067 ± 11 Ma	Cc-Cu±Dju±Bn±Ccp±Ag; Gnk±Sp±Gn±Wur	Chl	~100 - 150 °C	Pyrobitumen, petroleum, sour gas, in situ organic matter. Locally pyrite and chlorite.	Jones et al. (2023) Hitzman et al. (2005)

Table 3. Comparative table of the main features of sediment- and/ or volcanic-hosted Cu-Ag deposits worldwide. Mineral abbreviations are taken from Warr (2021). Abbreviations for gange minerals: Ab - Albite, Act - Actinolite, Anh - Anhydrite, Anl - Analcime, Cal - Calcite, Cb-Carbonate, Chl - Chlorite, Czo - Clinozoisite, Dol - Dolomite, Ep - Epidote, Kfs - K-felspar, Grt - Garnet, Ms - Muscovite, Lmt - Laumontite, Phl - Phlogopite, Pmp - Pumpellyite, Prh - Prehnite, Qz - Quartz, Rt - Rutile, Scp - Scapolite, Ser - Sericite, Ttn - Titanite, Tur - Tourmaline, Zeo – Zeolite. Abbreviations for ore minerals: Ag - Native Silver, Ani - Anilite, Ata - Atacamite, Azu - Azurite, Bn - Bornite, Bnr - Brannerite, Cli - Carrollite, Cc - Chalcocite, Ccl -Chrysocolla, Cth -Clausthalite, Ccp - Chalcopyrite, Cu - Native Copper, Cv - Covellite, Dg - Digenite, Dju - Djurleite, Gn - Galena, Gnk - Greenockite, Gth - Gothite, Hem - Hematite, Mlc - Malachite, Mol - Molybdenite, Py - Pyrite, Sp - Sphalerite, Spi - Spionkopite, Ttr-Tnt - Tetrahedrite-tennantite, Urn - Uraninite, Wur – Wurtzite.

Comparative analysis of Cu-(±Ag) mineralization in the "La Quinta" Formation and similar deposits worldwide

The stratabound Cu-(±Ag) deposits in the Perijá Range are hosted in a volcano-sedimentary pile containing continental, oxidized redbeds interlayered with subaerial, felsic to mafic flows (Maze, 1984; Jimenez, 2010). Similar hosting sequences are described for Volcanic Redbed Cu deposits and Chilean Mantos (Kirkham, 1984; Kojima et al., 2019). For instance, the Keweenaw district native Cu lodes, classified by Kirkham (1984) as a Volcanic Redbed Cu deposit, are hosted by tholeiitic basaltic flows and interflow conglomerates of the Portage Lake Volcanics unit (Brown, 2006; Bornhost et al., 1988). On the other hand, Chilean Manto-type deposits are predominantly hosted by bimodal volcanic rocks (basalt to rhyodacite) and minor sedimentary strata (Maureira et al, 2023, Kojima et al., 2019). Furthermore, the lithologies of the "La Quinta" Formation that host the mineralization are contrastingly different from those evidenced in Kupferschiefer-type deposits, in which ore minerals are associated with reduced-facies siliciclastic or dolomitic units of marine to lacustrine environments (Hitzman et al., 2005).

The hypogene mineralization in the "La Quinta" Formation mainly encompasses chalcocite, bornite, and, in minor amounts, native copper and native silver (Jimenez, 2010; González-Durán, 2016). Besides, as evidenced by the mineral chemistry assays, additional silver can also be hosted in Cu-sulfides. Despite some differences, overall ore content of Cu-(±Ag) deposits in the Perijá Range displays closer similarities to Volcanic Redbed Cu deposits, Chilean Mantos, and deposits such as White Pine and Keshtmahaki. The ore minerals at these deposits mainly include Cu-sulfides and/or native copper with silver-bearing phases (Bornhorst et al., 1988; Jones et al., 2023; Kirkham, 1984; Kojima et al., 2009; Jiba et al., 2021). By contrast, the "La Quinta" Formation ores do not include Cobalt, Uranium, Molybdenum, or Gold-bearing minerals, which are commonly found in the Central African Copper Belt (CACB) deposits (Hitzman et al.,2005; Selley et al., 2005; Jimenez, 2010). Additionally, there are no Lead or Zinc sulfides, which are common in Kupferschiefer-type deposits (Hitzman et al., 2005; Borg et al, 2012).

Regarding hydrothermal alteration, both Na-rich (albite ± quartz) and K-rich (K-feldspar – quartz) alteration assemblages might reflect the regional flow of non-mineralizing fluids through the "La Quinta" Formation. None of these are paragenetically associated with copper-silver ores. Then, zones with intense Na-rich and K-rich alterations do not indicate ore presence. Hitzman et al. (2005) associate the widespread occurrence of both alteration types with the basin-scale flow of diagenetic brines in the Katangan Supergroup of the CACB. There, intensely altered zones reflect a high rock-fluid interaction, however, they do not necessarily indicate ore presence since these alteration zones extend considerably beyond the orebodies (Hitzman et al., 2005). On the contrary, the Cu-(±Ag) mineralization at the "La Quinta" Formation occurs in paragenetic association with intense Ca-Si-rich alteration. Epidote-prehnite ± pumpellyite comprising this alteration might indicate a prograde low-grade (or burial) metamorphic environment for the mineralizing fluids genesis (Jimenez, 2010; Hitzman et al., 2005; Kirkham, 1984). These burial metamorphic conditions are further supported considering the significant thickness of the "La Quinta" Formation (1600 to 3000 meters) and the absence of penetrative deformation features (e.g. schistosity) related to regional (orogenic) metamorphism (Jimenez, 2010; Kirkham, 1984). Besides, the fluid inclusions temperatures obtained for the hypogene mineralization (100 to 260 °C) at the "La Quinta" Formation (González-Durán, 2016) would be in accordance with a low-grade metamorphic environment. Similar features were described for Volcanic Redbed Cu and Manto-type deposits. For instance, Portage Lake Volcanics in the Keweenaw district display mineral associations characteristic of subgreenshist conditions. The native Cu orebodies in this district overlie the pumpellyite-epidote transition zone (Kirkham, 1984; Hitzman, 1984; Brown, 2006; Jolly, 1974). On the other hand, Chilean Mantos host sequences have thicknesses of over 2 kilometers and were also subjected to burial or lower-greenschist metamorphism conditions (Kojima et al., 2009; Hitzman et al., 2005; Maureira et al., 2023; Herazo et al., 2020). On the contrary, Kupferschiefer-type deposits are not affected by metamorphism (Hitzman et al., 2005).

The mineralization styles in the study area encompass sediment-hosted and basalt-hosted deposits. In these settings, ore predominantly occurs as disseminations, vesicle fillings, and, to a lesser extent, as hydrothermal breccias and veinlets (González-Durán, 2016). Moreover, in the San Diego area, Jimenez (2010) also described the deposits as tabular bodies or lenses. Their dimensions vary from 2 to 10 meters in length and thicknesses of less than 1 meter. These orebodies are E-W striking structures with high-angle dips that crosscut the homoclinal host lithologies. Such characteristics support an epigenetic origin for mineralization and suggest that ore localization depends on lithological-sedimentological (i.e. permeability) and structural controls (i.e. fault zones) (Jimenez, 2010). Both are key since they allowed the fluid flow through the "La Quinta" Formation. Hitzman et al. (2005) and Kirkham (1984) described comparable ore localization controls for other sediment- and/or volcanic-hosted copper deposits, arguing that they reflect the basin architecture in which the mineralization occurred.

Additionally, the Cu-(±Ag) mineralization of the "La Quinta" Formation is related to in situ reductants. Semifusinite, pyrite, and plagioclase are in close spatial association with ore minerals. Then, they are suggested to be acting as "chemical traps" (González-Durán, 2016; Jimenez, 2010). Nevertheless, the possible occurrence of pyrobitumen with mineralization might also indicate that mobile reductants (i.e. hydrocarbons) could have acted as a key agent responsible for triggering ore precipitation. Despite further evidence being required for the Perijá Range orebodies, similar redox mechanisms have been described for deposits such as White Pine, Chilean Mantos (e.g. Lorena and El Soldado), and those belonging to the CACB (Hitzman et al., 2005; Jones et al., 2023; Herazo et al., 2020). According to the above, entrapment structures usually explored for hydrocarbons, such as structural (e.g. fault zones) and stratigraphic traps (e.g. pinch-outs) could also be potential targets for Cu-(±Ag) mineralization in the Perijá Range (Hitzman et al.,2005).

Table 3 summarizes the main characteristics of sediment- and/ or volcanic-hosed Cu-Ag deposits worldwide, including the Cu-(±Ag) deposits hosted by the "La Quinta" Formation at the Perijá Range.

Concluding Remarks

The Cu (±Ag) deposits hosted by the "La Quinta" Formation exhibit two distinct mineralization styles: Basalt-hosted and sediment-hosted mineralization. Basalt-hosted type is mainly formed by native copper and native silver, with minor amounts of Cu-sulfides. Silver can also exist as Cu-Ag alloys or within Cu-sulfides and Cu-Fe-sulfides. In contrast, the sediment-hosted mineralization comprises primary Cu-sulfides, including bornite, digenite, and chalcopyrite. As observed in basalts, Cu-sulfides and Cu-Fe-sulfides in sedimentary units also host traces of silver.

The identified hydrothermal stages include Na-rich, K-rich, Ca-Si-rich, and Ca-CO_2-rich alterations. The first alteration assemblage comprises albite + quartz, while the second includes K-feldspar + quartz. The third contains epidote + prehnite + chlorite + quartz, and the fourth is characterized by calcite + zeolite. Notably, the Cu (±Ag) mineralization is closely associated with the Ca-Si-rich alteration in the basaltic and sedimentary units. These mineral assemblages and lithogeochemistry vary according to host rock composition, suggesting that ore precipitation was influenced by the lithological features of the hosting units.

In sediment-hosted deposits, the ore minerals are spatially associated with charcoal clasts and possibly pyrobitumen. These forms of organic matter are possible sources of reduced sulfur, which may result in Cu-sulfides precipitation upon contact with mineralizing fluids. Conversely, the lack of sulfur-bearing minerals in basalts suggests that this lithology and/or the mineralizing fluids are sulfur-deficient.

Additionally, supergene oxidation has overprinted hypogene ores, forming secondary Cu-sulfides including spionkopite, anilite, and covellite. Other identified secondary Cu-bearing minerals are cuprite, tenorite, paramelaconite, delaffosite, malachite, azurite, and chrysocolla.

Acknowledgements

The authors thank the Colombian Geological Survey (Servicio Geológico Colombiano) for funding this research. The support from Leonardo Santacruz, Paola Rodríguez, and Carolina Jiménez with EPMA analyses is greatly acknowledged. William Chavez, Eric Petersen, Carlos Mario Celada, Celso Colombo Tassinari, and António Manuel Mateus are acknowledged for their kind field and conceptual assistance.

References

Alvarán, M., Naranjo, E., and Zapata, E. (2011). Skarn de cobre en la mina Río Frío, Payandé-Tolima: Aspectos mineralógicos, metalográficos y microtermométricos. Boletín de Ciencias de la Tierra, v. 29, p. 7–20.

Apergis, I., & Apergis, N. (2019). Silver prices and solar energy production. Environmental Science and Pollution Research. doi:10.1007/s11356-019-04357-1

Arias, A., Morales, C. (1999). Mapa geológico generalizado del Departamento del Cesar, Memoria explicativa, Ingeominas.

Bartos, P. J., Garcia, C., & Gil, J. (2017). The Nuevo Chaquiro Cu-Au-(Mo) Porphyry Deposit, Middle Cauca Belt, Colombia: Geology, Alteration, Mineralization. Economic Geology, 112(2), 275–294. doi:10.2113/econgeo.112.2.275

Bayona, G., Montes, C., Cardona, A., Jaramillo, C., Ojeda, G., Valencia, V., and Ayala-Calvo, C. (2011). Intraplate subsidence and basin filling adjacent to an oceanic arc-continent collision: a case from the southern Caribbean-South America plate margin. Basin Research, 23: 403–422.

Bird, D.K., Schiffman, P., Elders, W.A., Williams, A.E., McDowell, S.D. (1984). Calc-silicate mineralization in active geothermal systems. Economic geology, Vol. 79, 671- 695.

Borg, G., Piestrzyński, A., Bachmann, G.H., Puttman, W., Walther, S., Fiedler, M. (2012). An overview of the European Kupferschiefer deposits. Economic Geology Special Publication. Special Publication. 455-486.

Bornhorst, T., Paces, J., Grant, N., Obradovich, J., Huber, K. (1988). Age of native copper mineralization, Keweenaw Peninsula, Michigan. *Economic Geology*; 83 (3): 619–625. doi: https://doi.org/10.2113/gsecongeo.83.3.619

Brown, A.C. (2006). Genesis of Native Copper Lodes in the Keweenaw District, Northern Michigan: A hybrid Evolved Meteoric and Metamorphogenic Model. Economic Geology, 101(7), 1437–1444.

Brown, A. C. (2014). Low-Temperature Sediment-Hosted Copper Deposits. Treatise on Geochemistry, 251–271.

Cano, N.A. (2015). Petrografía y química mineral de los miembros volcánicos de la Formación La Quinta en los Andes nororientales de Colombia. Bachelor thesis, Universidad Nacional de Colombia, Bogotá.

Cardeño-Villegas, K., Rojas-Martínez, E.E., Manco-Jaraba, D.C., Cárdenas-López, R.R. (2015). Identificación de las Mineralizaciones de Cobre Aflorantes en el Corregimiento de San José de Oriente, La Paz, Cesar. Ingeniare, (18), 115–125. https://doi.org/10.18041/1909-2458/ingeniare.18.545

Cediel, F., Mojica, J., & Macía, C. (1981). Las formaciones Luisa, Payandé y Saldaña: sus columnas estratigráficas características. Geología Norandina, 3, 11-19.

Champetier de Riebes, G., Pagnacco, P., Radelli, L., Weecksteen, G. (1961). Geologia y mineralizaciones cupriferas de la Serrania de Perija, entre Becerril y Villanueva (Departamento del Magdalena, Intendencia de La Guajira): Boletín Geológico, v. XI, 1-3, p.133-188.

Chavez, W.X. (1990). Supergene Oxidation of Copper Deposits: Zoning and Distribution of Copper Oxide Minerals. SEG Newsletter N° 41, p. 10-21.

Church, C., Crawford A. (2020) Minerals and the Metals for the Energy Transition: Exploring the Conflict Implications for Mineral-Rich, Fragile States. In: Hafner M., Tagliapietra S. (eds) The Geopolitics of the Global Energy Transition. Lecture Notes in Energy, vol 73. Springer, Cham. https://doi.org/10.1007/978-3-030-39066-2_12

Colmenares, F., Mesa, A., Roncancio, J., Arciniegas, E., Pedraza, P., Cardona, A., Romero, A., Silva, C., Alvarado, S., Romero, O., Vargas, A. (2007). Geología de las planchas 11, 12, 13, 14, 18, 19, 20, 21, 25, 26,27, 33 Y 34. Proyecto: "Evolución Geohistórica De La Sierra Nevada De Santa Marta". Ingeominas.

Cornwall, H.R. (1956). A summary of ideas on the origin of native copper deposits: Economic Geology, v. 51, p. 615–631.

Easton, A. J., Hamilton, D., Kempe, D. R. C., & Sheppard, D. M. F. (1977). Mineralogy towards the Twenty-first Century. Philosophical Transactions of the Royal Society London, A., 253-71.

Forero, S. (1970). Estratigrafía del Precámbrico en el flanco occidental de la serranía de Perijá. Geología Colombiana, 7, 7-78.

Gablina, I.F., Mozgova, N.N., Borodaev, Y.S. (2004). Tetragonal form of Cu2S in recent hydrothermal ores of rainbow (Mid-Atlantic ridge, 36°14′ N), in Novye dannye o mineralakh(new data on minerals) 39, pp. 102–109 (Moscow).

Geoestudios. (2006). Cartografía geológica cuenca Cesar-Ranchería. Report.

Gómez, L. A., Buchely, F., Lancheros, J., Davila, C., Lopez, C., Romero, O., Gonzalez, F. (2010). Cartografía Geológica y Muestreo Geoquímico de la parte Norte de la Serranía de Perijá Plancha 21, 22, 27, 28, 34 y 35.

González, H., Maya, M., Camacho, J., Cardona, O. D., Vélez, W. (2015). Elaboración de la cartografía geológica de un conjunto de planchas a escala 1:100.000 ubicadas en cuatro bloques del territorio nacional, identificados por el Servicio Geológico Colombiano. Plancha 41: Becerril. Bogota: Servicio Geológico Colombiano.

González-Duran, A.F. (2016). Mineralogía, geoquímica y evolución de fluidos de una mineralización de cobre en Colombia. Bachelor thesis, Universidad Nacional de Colombia, Bogotá.

Hayes, T.S., Cox, D.P., Piatak, N.M., and Seal, R.R., II. (2015), Sediment-hosted stratabound copper deposit model: U.S. Geological Survey Scientific Investigations Report 2010–5070–M, 147 p. http://dx.doi.org/10.3133/sir20105070M

Hatert, F. (2005). Transformation sequences of copper sulfides at Vielsalm, Stavelot Massif, Belgium. The Canadian Mineralogist, 43 (2): 623–635. https://doi.org/10.2113/gscanmin.43.2.623

Henley, R.W., Ellis, A.J. (1983). Geothermal systems Ancient and Modern: A geochemical review. Earth-Science Review, 19: 1-50.

Herazo, A., Reich, M., Barra, F., Morata, D., del Real, I., Pagès, A. (2020). Assessing the role of bitumen in the formation of stratabound Cu-(Ag) deposits: Insights from the Lorena deposit, Las Luces district, northern Chile. Ore Geology Reviews, 103639. doi: 10.1016/j.oregeorev.2020.103639

Hernández, M. (2003). Memoria explicativa geología plancha 48, Jagua de Ibirico. Esc 1:100.000. Bogotá. Ingeominas.

Hitzman, M., Selley, D., Bull, S. (2010). Formation of Sedimentary Rock-Hosted Stratiform Copper Deposits through Earth History. *Economic Geology*; 105 (3): 627–639. doi: https://doi.org/10.2113/gsecongeo.105.3.627

Hitzman, M., Kirkham, R., Broughton, D., Thorson, J., Selley, D. (2005). The Sediment-Hosted Stratiform Copper Ore System, One Hundredth Anniversary Volume, Jeffrey W. Hedenquist, John F. H. Thompson, Richard J. Goldfarb, Jeremy P. Richards

IEA. (2021). The Role of Critical Minerals in Clean Energy Transitions, IEA, Paris, https://www.iea.org/reports/the-role-of-critical-minerals-in-clean-energy-transitions, Licence: CC BY 4.0

Ikehata, K., Chida, K., Tsunogae, T., Bornhorst, T.J. (2016). Hydrothermal native copper in ocean island alkali basalt from the Mineoka belt, Boso peninsula, central Japan. Economic Geology, 111(3). 783–794. https://doi.org/10.2113/econgeo.111.3.783

Jiba, Z., Ghaderi, M., Maghfouri, S. (2021). Geology, mineralogy and fluid inclusion studies of the Yamaghan Manto-type Cu (Ag) deposit, southeast Zanjan, NW Iran. 11. 594-615. 10.22055/aag.2021.34764.2157.

Jiménez, C. (2010). Vulcanismo y Manifestaciones cupríferas de la Serranía de Perijá. Bachelor thesis, Universidad Nacional de Colombia. Facultad de Minas, Medellín.

Jolly, W.T. (1974). Behaviour of Cu, Zn, and Ni during prehnite-pumpeliyite rank metamorphism of the Keweenawan basalts, northern Michigan; Economic Geology, vol. 69, p. 1118-1125.

Jones, S., Cloutier, J., Prave, A., Raub, T., Stüeken, E., Stein, H., Yang, G., Boyce, A. (2023). Fluid Flow, Alteration, and Timing of Cu-Ag Mineralization at the White Pine Sediment-Hosted Copper Deposit, Michigan, USA. *Economic Geology*; 118 (6): 1431–1465. doi: https://doi.org/10.5382/econgeo.5013

Kammer, A., Mojica, J. (1995). Eventos Jurásicos en Colombia. Geología Colombiana, 19, p. 165-172.

Kirkham, R.V. (1984). Volcanic Redbed Copper; in Canadian Mineral Deposit Types, A Geological Synopsis, Eckstrand, O.R., Editor. Geological Survey of Canada, no 8, p. 241-252.

Kojima, S., Trista-Aguilera, D. and Hayashi, K.-i. (2009). Genetic Aspects of the Manto-type Copper Deposits Based on Geochemical Studies of North Chilean Deposits. Resource Geology, 59: 87-98. https://doi.org/10.1111/j.1751-3928.2008.00081.x

Konari, M., Rastad, E., Kojima, S., Omran, N. (2013). Volcanic redbed-type copper mineralization in the Lower Cretaceous volcano-sedimentary sequence of the Keshtmahaki deposit, southern Sanandaj-Sirjan Zone, Iran. Neues Jahrbuch für Mineralogie - Abhandlungen. 190. 107-121. doi: 10.1127/0077-7757/2013/0236.

Lobo-guerrero, A. (2003). Gold and copper dissemination in the igneous-volcanic Saldaña Formation, Natagaima, Tolima, Colombia, and extension of the mineral province in the Andean Cordillera. Proccedings 10° congreso geológico chileno. https://biblioteca.sernageomin.cl/opac/DataFiles/LoboGuerreroA1.pdf

Mahdavi, A., & Rajabi, A. (2023). Neotocite textures as a clue to the exploration of Red Bed type sediment-hosted stratabound copper (SSC) deposits–evidence from Ravar–Tabas–Eshghabad copper belt, Central Iran. International Geology Review, 1-15. https://doi.org/10.1080/00206814.2023.2241069

Mahecha, L.F., & Zuluaga, C., A. (2016). Geochemical and Petrographic Analysis of a Copper Sediment-Hosted Mineralization at Chiquinquirá Village, Boyacá Department, Colombia. Proceedings of the Society of Economic Geologists conference, Turkey.

Manco-Jaraba, D.C., Ariño-Díaz, K.R., Rojas-Martínez, E.E. (2019). Prospection and characterization of copper deposit in Los Cueros village, Villanueva, La Guajira's department-Colombia. Ingeniare. Revista chilena de ingeniería, 27(2), 288-294. https://dx.doi.org/10.4067/S0718-33052019000200288

Manco, J. D. (2020). Geology, geochronology and geochemistry of the El Alacrán Deposit, San Matías District, Cordoba-Colombia (T). University of British Columbia. Retrieved from https://open.library.ubc.ca/collections/ubctheses/24/items/1.0390466

Maureira, I., Barra, F., Reich, M., Palma, G. (2023) Geology of the Altamira and Las Luces deposits, Coastal Cordillera, northern Chile: implications for the origin of stratabound Cu–(Ag) deposits. *Miner Deposita* 58, 379–402. https://doi.org/10.1007/s00126-022-01132-0

Maze, W.B. (1984). Jurassic La Quinta Formation in the Sierra de Perija, northwestern Venezuela: Geology and tectonic environment of red beds and volcanic rocks. Geological Society of America, memoir 162.

Miller, J.B. (1962). Tectonic trends in Sierra de Perija and adjacent parts of Venezuela and Colombia. AAPG Bull., 46: 1565-1595.

Movahednia, M., Maghfouri, S., Fazli, N., Rastad, E., Ghaderi, M., González, F. (2022). Metallogeny of Manto-type stratabound Cu-(Ag) mineralization in Iran: Relationship with NeoTethyan evolution and implications for future exploration, Ore Geology Reviews, Volume 149, 105064, ISSN 0169-1368, https://doi.org/10.1016/j.oregeorev.2022.105064.

Murillo-Bedoya, J.M. (2020). Petrographic and litho-geochemical characterization of the VMS deposit at El Roble mine, Colombian Western Cordillera. Bachelor thesis, EAFIT university. https://repository.eafit.edu.co/bitstream/handle/10784/24651/Murillo%20J.M%202020.pdf?sequence=2&isAllowed=y

Nova, G., Montaño, P., Bayona, G., Rapalini, A., & Montes, C. (2012). Paleomagnetismo en rocas del Jurásico y Cretácico Inferior en el flanco occidental de la serranía del Perijá: contribuciones a la evolución tectónica del NW de Suramérica. Boletín de Geología, 34 (2), 117-138.

Ortega, C.R., Rojas, E.E., & Manco-Jaraba, D.C. (2012a). Mineralización de cobre en el sector de San Diego, Serranía del Perijá. Geología Colombiana, 37. https://revistas.unal.edu.co/index.php/geocol/article/view/22409

Ortega, C.R., Rojas, E.E., & Manco-Jaraba, D.C. (2012b). Depósitos estrato confinados de cobre en el municipio de San Diego, Cesar, Serranía del Perijá. Revista Prospectiva, Vol. 10(1), pp. 28-36.

Pagnacco, P. (1963). Cupriferous Mineralizations in the Serranía de Perijá between Codazzi and Molino. Geología Colombia No 2: 5-13 p. Bogotá.

Pastor-Chacón, A., Reyes-Abril, J., Cáceres-Guevara, C., Sarmiento, G., Cramer, T. (2013). Análisis estratigráfico de la sucesión del Devónico-Pérmico al oriente de Manaure y San José de Oriente (serranía del Perijá, Colombia). Geología Colombiana, 38, 5-24.

Pinto, V.M., Hartmann, L.A., and Wildner, W. (2010). Epigenetic hydrothermal origin of native copper and supergene enrichment in the Vista Alegre district, Paraná basaltic province, southernmost Brazil: International Geology Review, v. 53, p. 1163–1179.

Radelli, L. (1962). Acerca de la geología de la Serranía de Perijá entre Codazzi y Villanueva. Geología Colombia No 1: 21-41 p. Bogotá.

Ramírez, L.E., Palacios, C., Townley, B. *et al.* (2006). The Mantos Blancos copper deposit: an upper Jurassic breccia-style hydrothermal system in the Coastal Range of Northern Chile. *Miner Deposita* 41, 246–258. https://doi.org/10.1007/s00126-006-0055-9

Rodríguez, S.E. (1986). Génesis y mineralogía de los depósitos de cobre del Táchira nororiental, Venezuela. Geología colombiana, No. 15, pp. 177-184.

Rodríguez-García, G., Obando, G. (2020). Volcanism of the La Quinta Formation in the Perijá mountain range. Boletín Geológico, (46), 51-94. https://doi.org/10.32685/0120-1425/boletingeo.46.2020.535

Rodríguez-Madrid, A.L., Bissig, T., Hart, C.J.R., & Mantilla-Figueroa, L.C. (2017). Late Pliocene High-Sulfidation Epithermal Gold Mineralization at the La Bodega and La Mascota Deposits, Northeastern Cordillera of Colombia. Economic Geology, 112(2), 347–374. doi:10.2113/econgeo.112.2.347

Sadati, S.N., Yazdi, M., Mao, J., Behzadi, M., Adabi, M. H., Lingang, X., Mokhtari, M.A.A. (2016). Sulfide mineral chemistry investigation of sediment-hosted stratiform copper deposits, Nahand-Ivand area, NW Iran. Ore Geology Reviews, 72, 760–776. doi: 10.1016/j.oregeorev.2015.09.018

Selley, D., Broughton, D., Scott, R., Hitzman, M., Bull, S., Large, R., McGoldrick, P., Croaker, M., Pollington, N., Barra, F. (2005). A New Look at the Geology of the Zambian Copperbelt, One Hundredth Anniversary Volume, Jeffrey W. Hedenquist, John F. H. Thompson, Richard J. Goldfarb, Jeremy P. Richards

Shaw, R.P. (2014). VHMS- and sediment-hosted base metal occurrences in the Colombian Cordilleras. https://app.ingemmet.gob.pe/biblioteca/pdf/CPG17-117.pdf

Shaw, R.P., Leal-Mejía, H., Melgarejo i Draper, J.C. (2019). Phanerozoic Metallogeny in the Colombian Andes: A Tectono-magmatic Analysis in Space and Time. In: Cediel, F., Shaw, R.P. (eds) Geology and Tectonics of Northwestern South America. Frontiers in Earth Sciences. Springer, Cham. https://doi.org/10.1007/978-3-319-76132-9_6

Sillitoe, R.H. (2018). Comments on Geology and Exploration Potential of the San Matias Project, Colombia, A report prepared for Cordoba Minerals Corp., 1-15.

Sillitoe, R.H. (2008). Special Papel: Major Gold Deposits and Belts of the North and South American Cordillera: Distribution, Tectonomagmatic Settings, and Metallogenic Considerations. Economic Geology, 103(4), 663-687. doi: https://doi.org/10.2113/gsecongeo.103.4.663

Sillitoe, R. H., Jaramillo, L., Damon, P. E., Shafiqullah, M., & Escovar, R. (1982). Setting, characteristics, and age of the Andean porphyry copper belt in Colombia. Economic Geology, 77(8), 1837–1850. doi:10.2113/gsecongeo.77.8.1837

Tschanz, C., Jimeno, A., & Cruz, J. (1969). Geology of the Sierra Nevada de Santa Marta area, Colombia. Informe interno 1829. Bogotá: Ingeominas.

Ujueta, G., Llinás, R. (1990). Reconocimiento Geológico de la parte más Septentrional de la Sierra de Perijá. Geología Colombiana, 17, 197-209. https://revistas.unal.edu.co/index.php/geocol/article/view/30670

Vaughan, D. J., Sweeney, M. A., Friedrich, G., Diedel, R., Haranczyk, C. (1989). The Kupferschiefer; an overview with an appraisal of the different types of mineralization. *Economic Geology*; 84 (5): 1003–1027. doi: https://doi.org/10.2113/gsecongeo.84.5.1003

Viteri, E. (1978). Génesis del Cobre Nativo asociado a Rocas Volcánicas de la Formación la Quinta-Perijá, Venezuela. Boletín de Geología. Vol. 13(24), pp. 47-82.

Warr, L. N. (2021). IMA–CNMNC approved mineral symbols. *Mineralogical Magazine*, *85*(3), 291–320. doi:10.1180/mgm.2021.43

Wilkinson J.J. (2014) Sediment-Hosted Zinc–Lead Mineralization. In: Holland H.D. and Turekian K.K. (eds.) Treatise on Geochemistry, Second Edition, vol. 13, pp. 219-249.

Wilson, N., Zentilli, M. (1999). The role of organic matter in the genesis of the El Soldado Volcanic-Hosted Manto-Type Cu Deposit, Chile. Econ. Geol. 94, 1115–1136.

Wilson, N., Zentilli, M. (2006). Association of pyrobitumen with copper mineralization from the Uchumi and Talcuna districts, central Chile. Int. J. Coal Geol. 65 (1),158–169.

Wokittel, R. (1957). Formación cuprífera de la Serranía de Perijá intendencia de La Guajira y Departamento del Magdalena. Informe 1193, 35 p. Servicio Geológico Nacional, Bogotá.